CZECH TECHNICAL UNIVERSITY IN PRAGUE

Diaphragm Postural Function Analysis using Magnetic Resonance

Pavel Vostatek

in the

Faculty of Electrical Engineering

Department of Cybernetics

May 2010

Abstract

We present postural analysis of diaphragm function using magnetic resonance imaging (MRI). The main aim of the current study is to identify changes of diaphragm motion and shape. 16 healthy subjects are compared to 17 subjects suffering from chronic pain and having structural spine findings. Two sets of features are calculated from MRI recordings: i) dynamic parameters reflecting diaphragm action and ii) static parameters. Statistical analysis show that diaphragm respiratory and postural changes are significantly slower, bigger in size and better balanced in control group. Furthermore, a classification analysis between subject with and without chronic pain was carried out yielding sensitivity 0.97, specificity 1.0 and classification error 0.014 using normal densities based linear classifier.

Abstrakt

Práce se zabývá parametrizací pohybu a polohy bránice na obrázcích magnetické rezonance. Dynamická magnetická rezonance byla použita nasnímání 20 s sekvencí dechu pro skupinu zdravých probandů a zároveň pro skupinu lidí trpících bolestí zad s potvrzeným strukturálním nálezem na páteři. Naším kolem bylo vytvořit sadu parametrů, pro charakterizaci jednak polohy, tvaru a náklonu bránice. A také pro charakterizaci jejího pohybu. Následovalo statistické vyhodnocení parametrů bránice. To prokázalo statisticky signifikantní rozdíly ve frekvenci dechu a také hloubce nádechu. Statistické rozdíly se vyskytly i v případě statických parametrů. Výška bránice a její náklon se signifikantně lišila mezi skupinami.

V rámci práce byly použity pojmy, které jsou nové v kontextu zpracování dechových sekvencí. Parametry hodnotící pohyb bránice (hodnocení harmoničnosti dechu, použití statistických momentů přímo na průběh dechu) jsou zatím ojediněle použité v medicínském kontextu.

Acknowledgements

My biggest word of thanks goes to my advisor Daniel Novák for his many valuable remarks and kind lead through the thesis developement. I would also like to send big thank to my parents for their support and love. Without them this work would never came to existence. I also greatly appreciate all my friends and wish them the best.

České vysoké učení technické v Praze
Fakulta elektrotechnická

Katedra kybernetiky

ZADÁNÍ DIPLOMOVÉ PRÁCE

Student: Bc. Pavel V o s t a t e k

Studijní program: Elektrotechnika a informatika (magisterský), strukturovaný

Obor: Biomedicínské inženýrství

Název tématu: Diagnostika posturálních poruch
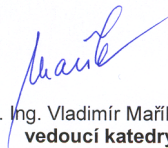
Pokyny pro vypracování:

1. Seznamte se s problematikou vyhodnocování stabilizace pohybu.
2. Navrhněte metodu pro objektivní diagnostiku posturálních poruch.
3. Evalujte navržený přístup na kontrolní skupině a na skupině pacientů.

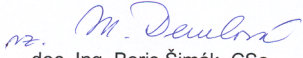**Seznam odborné literatury:**

Müller, O.; Günther, M.; Krauss, I.; Horstmann, T.: Physical Characterization of the
Therapeutic Device Posturomed as a Measuring Device--Presentation of a Procedure
to Characterize Balancing Ability. Biomed Tech (Berl). 2004 Mar;49(3):56-60.

Vedoucí diplomové práce: Ing. Daniel Novák, Ph.D.

Platnost zadání: do konce zimního semestru 2009/2010

prof. Ing. Vladimír Mařík, DrSc.
vedoucí katedry

L.S.

doc. Ing. Boris Šimák, CSc.
děkan

V Praze dne 3. 9. 2008

Prohlášení

Prohlašuji, že jsem svou diplomovou práci vypracoval samostatně a použil jsem pouze podklady (literaturu, projekty, SW atd.) uvedené v přiloženém seznamu.

V Praze dne ……14.5.2010…….   ………………Pavel Vosýšeš………
                                                                                    podpis

Contents

List of Figures

List of Tables

Abbreviations

FFT   Fast fourier transform

MRI   Magnetical resonance imaging

FISP   MRI Fast imaging with steady state precession

NSA   The average number for each phase encoding step

TR   Repetition time

TE   Echo delay time

FA   Fractional anisotropy

TSE   Turbo spin echo

FOV   Field of view

GUI   Graphical user interface

Symbols

a_t	Area characterizing diaphragm movement	$[cm^2]$
C_1, C_2	Healthy resp. pathological proband group	
S_A, S_B, S_C	Measured situations: A, B, C	
P_m	Point leid in center of a diaphragm contour	
I_B	Image with the diaphragm in caudal position	
Di_t	Difference image I_t (t-th image) and I_B subtracted	
t_s	Sagittal size of a thorax.	[mm]
f_r	Frequency of a res-curve	[Hz]
a_r	Amplitude of a res-curve	[-]
f_p	Frequency of a res-curve	[Hz]
a_p	Amplitude of a res-curve	[-]
r_{rs}	Amplitudes ratio of res- and pos-curve	[-]
p_3	The percentage of energy yielded by the three largest spectrum lines	[%]
dec_a	Diaphragm declination in sagittal plane in caudal position	[°]
dec_r	Diaphragm declination in sagittal plane in cranial position	[°]
b_i	i=1,..,5, partial height of a diaphragm in 5 different points	[-]
vd_6	Vertical distance from point b_5 and back marker (syrenge)	[-]
e_d	Eccentricity of an ellipse fitted to a diaphragm contour	[-]
c_d	Relative position of the highest point of a diaphragm	[-]
h_d	Height of a strip overlapping diaphragm contour	[-]
σ_{DC}	Standard deviation of a breath curve	[-]
γ_{DC}	Skewness of a breath curve	[-]
β_{DC}	Kurtosis of a breath curve	[-]
α_2	Angle of between the ventral part of diaphragm and the horizont	[°]

α_6 Angle of between the dorsal part of diaphragm and the horizont   [°]

δ Angle between a line fitted to the diaphragm contour and the horizont   [°]

$\rho_d.$ Diameter of a circle fitted to a diaphragm contour   [-]

Dedicated to gophers.

Chapter 1

Introduction

1.1 Motivation

This work deals with technical aspects of research pursuing changes in diaphragm motion, shape and position for patients suffering from chronic pain and having structural spine finding. The work proposed is based on study accomplished by Mgr. Tomáš Rychnovský as his doctoral degree thesis on Faculty of Physical Education and Sport, Charles University — [1].

Because diaphragm serves as an important postural stabilisation muscle, previous work focused on changes in its shape and position during miscellaneous illnesses occurences (see sec. 1.2). We extended this field by contributing actual state of art of diaphragm behaviour while patient suffers from structural spine finding. Rychnovský brought up medical hypotheses (section 1.2) and colleceted data (dynamical magnetic resonance was used for diaphragm motion scanning). Our goal was to deal with image sequence processing, extract data characterizing breath course and statical characteristic of diaphragm (introduced in sec. 3.1 and the particular features extracted are described in sec. 4.1 then).

1.2 Medical basics

Diaphragm besides function as a respiration muscle also works as an important stabilisation part of a body. Diaphragm and stabilisation trunk muscles are described as important functional unit of dynamic stabilisation of backbone. Its cooperation dysfunction is considered as one of the main factors evoking vertebrogenial problems and

causing structural spine finding also. Studies dealing with diaphragm are mainly focused on its respiration function. List of medical studies dealing with this theme are listed in [1]. Till now, diaphragm was studied in different types of strain (like pressure on lower limbs) on healthy probands only. This work as first expanded studied group by vertebrogenial patients. Group of healthy and unhealthy probands was compared to each other to make deductions of diaphragm changes while bad postural function is pursued.

1.3   Technical basics

Dynamic magnetic resonance imaging (MRI) was used for image acquisition (see sec. 2.1 for details). Technical processing described in this thesis was done in programming environment Matlab 2008 devoleped by The Mathworks. For classification part of research PRTools for Matlab were used ([2], http://www.prtools.org/). Our part of the work embraced image processing (characterization of diaphragm movement, diaphragm shape and position), extraction of devised features, statistical evaluation of inter-group feature differences and developement of classification framework with its tests and possibilities of automatic patient subsumption. Also graphical user interface was developed for visual data inspection... 3.3. Short description of work intention follows. Detailed description of course and results of our research are described in respective sections 2.1 for data acquisition details, 3.1 for data processing details, 4.1 for extracted parameters details and 5.1.1 for their limitations and at the end we investigated possibilities of patient classification in 6.

1.3.1   MRI usage background

Magnetic resonance imaging has been valuable in the assessment of abnormalities related to the diaphragm, mainly because it allows for direct and sagittal imaging. According to [1]. Gierada et al. [3] described diaphragmatic motion in normal subjects using sequential magnetic resonance images taken during quiet breathing, and Gauthier et al. [4] evaluated the shape of diaphragm at different lung volumes. Cluzel et al. [5] obtained fast three dimensional (3D) MRI during short periods of breath-holding, and the reconstructed images were used to measure the diaphragmatic area as well as changes in this area with respect to lung volume. Suga et al. [6] reported asynchronous movement between the ribcage and diaphragmatic motion by measuring the anteroposterior distance at the upper and lower thorax on sequential MRI. Others work are dedicated to measure diaphragm physiological main characteristics as height [7] or excursion [8].

However, there are few works inspecting postural functions during respiration or diaphragm activation during breath-holding [9]. To our knowledge, there is no similar work dedicating to postural diaphragm function in pathological cases.

1.3.2   Image processing

Image processing was composed of automatic and manual part. Automatic processing consisted of breath course characterisation done by introducing a breath-curve describing diaphragm movement (section 3.1). This section was inspired by previous work done by Kolář ([9]). Manual part of image processing consisted of inserting diaphragm contour onto images representing the lowest and the highest diaphragm position in trunk (see sec 3.2.1). All features which were devised and thought to be informatively worthwhile were computed from these data.

1.3.3   Statistical evaluation

After obtaining the features characterizing every patient, the values were examined and compared between the subjected groups. Simple statistical t-test was used to rate proband group differencies. Statistical significance of mean values distance of every feature was thereby estimated — see section 5.2. Physiological meaning of these results was than done by Tomáš Rychnovský in his work [1].

1.3.4   Classification framework

Experimets with selecting usable subset of information supporting features and automatic patient classification to healthy or painful group were processed. We tried to use different classifiers and different feature selection methods. Our goal was to find the most informative feature subset for classification. Also some deductions for these subsets and its respective features was set up to be eventually discussed in subsequent works.

1.3.5   Graphical user interface

Graphical user interface (GUI) was completely developed in Matlab. It's purpose is to explore obtained MRI images and most importantly to input desired values (1.3.2) for further processing. It allows one to explore input data and consequently computed statistics of features.

Chapter 2

Data acquisition and description

2.1 Data acquisition

2.1.1 Proband groups

We had two groups of probands to examine.

- **Group 1** (C_1): consisted of 16 people without a pathological condition. There were 11 women, 5 men. None of subjects had any pulmonary disease and/or serious spinal complaints. The average age was 35 years (range from 23 to 56 years).

- **Group 2** (C_2): consisted of 17 peple with pain present in a back and with structural spine finding. Composed of 8 women and 9 men. Structural findings of pathological group were confirmed by MRI imaging in the L-p spine area. Subjects suffered from chronic paint of different frequency and intensity determined by visual analog pain scale. The average age was 42 years (age range from 23 to 65 years).

Detailed informations are summarized in table 2.1. All volunteers were informed of the purpose of the study and the methods used prior to giving their written consent. The study was conducted according to local ethical and legal regulations. Diaphragm activity was monitored under tidal breathing.

TABLE 2.1: Details of studied groups (mean ± standard deviation).

Group	age	weight (kg)	height (cm)	sternum height (cm)	thorax height(cm)
C1	35 ± 11	71 ± 15	172 ± 10	20.9 ± 1.61	30 ± 2.1
C2	42 ± 11	78 ± 16	174 ± 6	21.4 ± 1.77	30.2 ± 1.7

No significant differences between proband groups in basic parametrs were verified by t-test. It prove that probands were selected properly and no significant differencies were present on significance level of 0.05. See 2.2 for results:

TABLE 2.2: T-test result to except significant inter class differences. Result 0 means mean values of compared sets are the same and 1 means they differ.

Test	age	weight (kg)	height (cm)	sternum height (cm)	thorax height(cm)	BMI	lower ribcage perimeter (cm)
T-test result	0	0	0	0	0	0	0
T-test p-value	0.076	0.646	0.225	0.160	0.077	0.792	0.486

2.1.2 MR settings

- **C1:** open MRI apparatus from Siemens, with a 0.23 T magnet and the software load version NUMARIS/4 syngo MRI 2004A.

  Each recorded sequence: 20 s, 77 images at regular intervals = one image acquired every 260 ms.

  The width of each layer: 33 mm.

  We have used true FISP dynamic sequence configured as follows: 1 NSA, matrix 240x256 pixels, TR 4.48 ms, TE 2.24 ms, FA 90°, TSE1, FOV 328 mm.

  Resolution: 1.37 mm/pixel.

- **C2:** MRI by General Electric, SIGNA HDx, with a 1.5 T magnet and the software load version 14-M5A.

  Each recorded sequence: 22.2 s, 60 images at regular intervals = one image acquired every 370 ms.

  The width of each layer was 15 mm.

  We have used GE FIESTA Cine dynamic sequence configured as follows: 1 NSA, matrix 256x256 pixels, TR 3.1 ms, TE 1.3 ms, FA 55°, FOV 420 mm.

  Resolution: 1.64 mm/pixel.

Acquired images were stored in DICOM format. For our work are images always processed as classic bitmaps and due to processing procedure, resortation from initial folder structure was done so after it every single proband had his images in folder to work with (see sec. 2.3 for details and 3.3 for GUI implementation).

For both proband groups the diaphragm was projected in the sagittal plane with the subject in a supine position, using a size large body coil. The projection plane was

placed sagittally in the axial topogram directed through paravertebrally on the right side, midway through the center of the vertebral body and the edge of the thoracic wall.

Three markers, 20-ml syringes filled with water, were placed on the skin surface of each subject on his right side. They are shown as hyper signal circles on the body surface (see for example figure 2.1). The first marker was placed in the mid-clavicular line at the level of jugular opening, the second at the level of the inferior 10-rib costal margin. The last marker was placed on the subjects back at the level of the thoracolumbar junction.

Due to image different resolution our proposed processing methodology was developed to be indifferent to distinct images resolution.
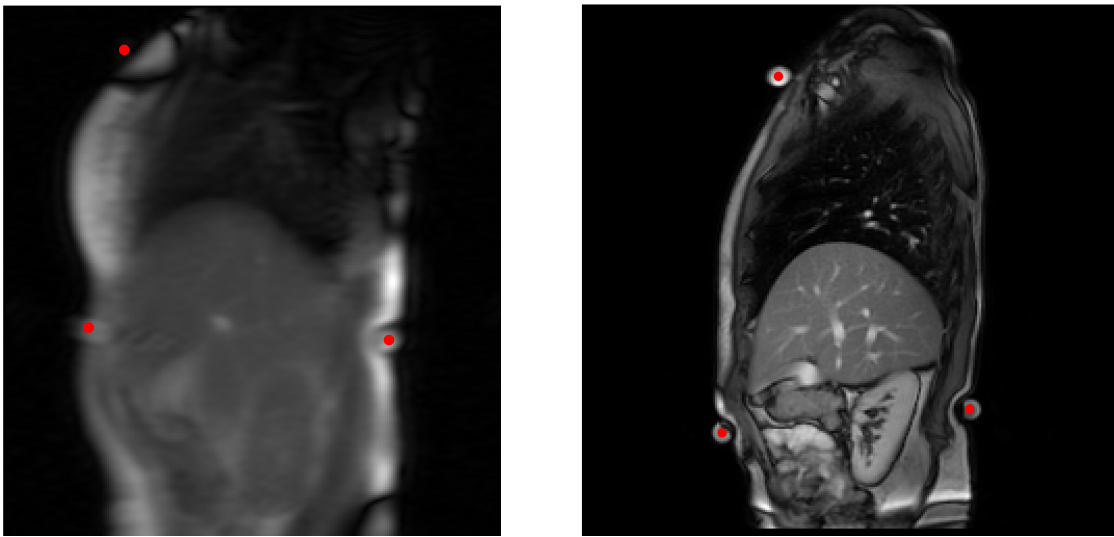
FIGURE 2.1: This figure shows example of output of both MR devices. There is image of C_1 on the left and C_2 on the right. As you can see due to lower magnetic power of used device for C_1 imaging there are less details though image resolution is bigger. Still desired diaphragm margins are visible quite good on both images. Still this issue should be kept in mind while evaluating results and could cause some inaccuracy.

2.2   Data structure

Besides calibration images for every proband 3 main breath cycles were present in MR image sets. These were:

- **Situation A** (S_A): Sequences of diaphragm were recorded while normally breathing.

- **Situation B** (S_B): Sequences of diaphragm were recorded while normally breathing but pressure against lower limbs was present. For deatils of this pressure settings see [1].

- **Situation C** (S_C): Sequences of diaphragm were recorded while holding breath and also pressure against lower limbs present. In this work S_C is processed as a single image as diaphragm was taken as still.[1]

2.3   Data sorting

Obtained data were in DICOM format. Information about data structure was only present in one info file. A special viewer was enclosed with every package of data and we weren't able to find any universal viewer to view all data at once.

Thus we decided to rearrange image files to folder structure corresponding with its division onto measured probands and furthermore on particular measured situations $S_A..S_C$. Final strucutre of working data follows:

- \<data directory\>
  - \<subdata dir. (healthy group) - optional\>
    * \<patient 1's name\>
      · \<measurement 1s name\>
        ⋮
        measurement files
        ⋮
      · \<measurement 2s name\>
        ⋮
    * \<patient 2s name\>
      ⋮
    * \<patient ns name\>
  - \<subdata dir. (painful group) - optional\>
    * \<patient (n + 1)s name\>
    * \<patients (n + 2)s name\>
      ⋮
    * \<patients ms name\>

---

[1]First we worked with this situation only as static image. Later on we realized some movement of the diaphragm is also present in these sequences even if it should not be respiration movement though. In our work we present methods of features computation which can be used on every situation so we do not present results of dynamic features of S_C as they were done after closing this part of our work and this work isn't primarily focused on medical conclusions.

The observed proband groups had different tags in DICOM file header filled in thus different tags were used for files sorting. Sorting procedure consisted of creating a directory for every unique patient in the data set and moving files of this patient into the directory. Then rename of the data files as per some tags characterizing time of image acquisition and sequence number followed. Moving proband files into designated folder was done automatically by Matlab script and redistributing each proband's files into sequences was done manually then.

Group C_1 files were named after tag `AcquisitionTime`.
Group C_2 files were named by `SeriesDescription`, `SeriesNumber` and `InstanceNumber`.

Chapter 3

Data processing

3.1 Desired information & its extraction

First, we extracted the following information from diaphragm images. Information characterizing diaphragm's position and shape:

1. `Diaphragm rotation.`

2. `Diaphragm flatness and height.`

3. `Diaphragm position in a trunk.`

4. `Diaphragm shape (its bow and changes in this profile).`

These parameters served for defining static parameters which are described in section 4.1.

Information characterizing diaphragm motion:

1. `Breath frequency.`

2. `Depth of breathe in.`

3. `Dominant position of diaphragm during breathing.`

4. `Possible changes of diaphragms average position.`

These extracted parameters would form set of dynamical features which are later described also in 4.1.

For extraction of properties listed above we needed a method to characterize diaphragm motion. Kolář proposed method for summarizing diaphragm motion in [9]. We define c_l as diaphragm in its lowest position and c_t the diaphragm in position we are currently inspecting. Then aim of our method is to measure area bordered by c_l and c_t for every image in a sequence. Area was labeled a_t where $t = 1..n$, n is the number of images in processed sequence. By displaying a_t as a time function we obtain curve which characterize diaphragm motion. Its sample shown in fig 3.1.
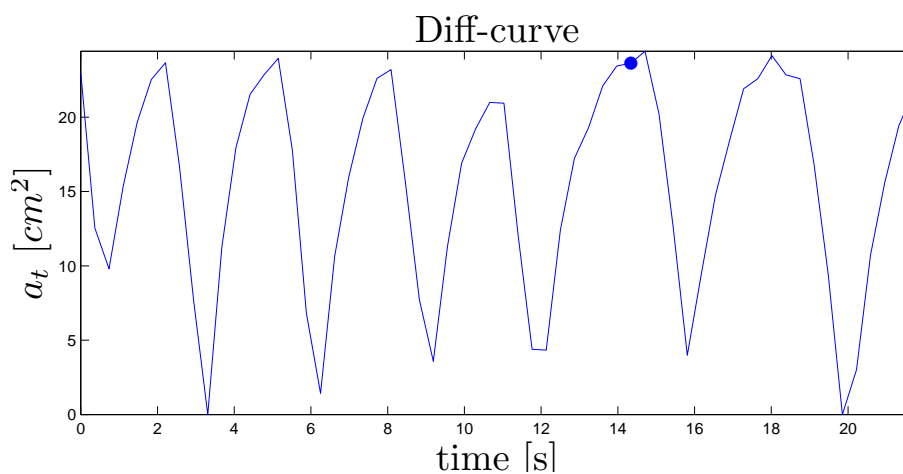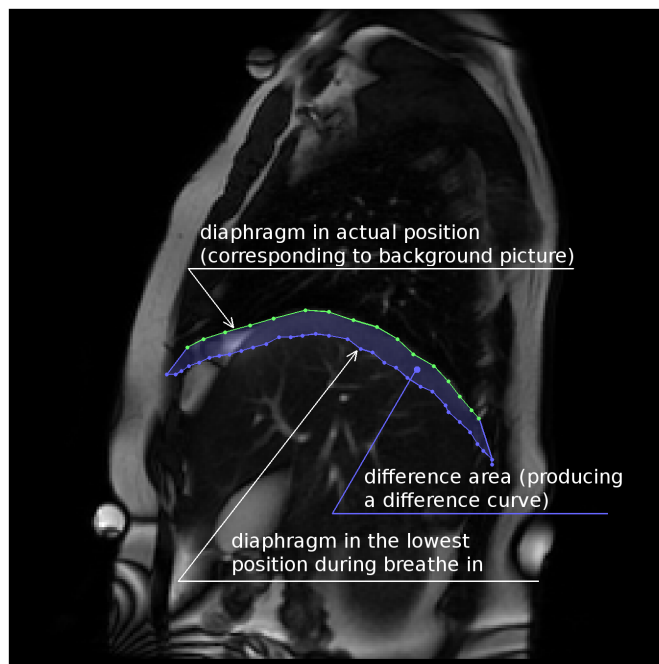
FIGURE 3.1: We obtain breath-curve as result of measuring area bordered by diaphragm contours in the lowest position on bottom and actual position on top in time (upper image). Breath-curve from proband shown on upper image with point illustrating a_t displayed on upper image.

Most desired breath-curve property is that it follows diaphragm motion such as when diaphragm goes up than breath-curve rises (when proband is breathing out). We suppose normal breath mostly harmonic and presume breath-curve harmonic also. Figure 3.1 shows that for harmonic breath the curve is also harmonic. We can see desired informations are present in graph in lower part of figure 3.1. Breath-curve is harmonic having main average frequency (breath frequency) and an amplitude (breath depth). Also dominant position of diaphragm and average position changes are visible. Methodology of breath-curve processing is described in section 3.4.1.

3.2 Manual input values and our approach to breath-curve computation

3.2.1 Input data

For proper diaphragm processing several input values were inserted manually:

- A point layed in the middle of diaphragm contour. It is inserted only in the first image of sequence. viz image 3.2. Denoted P_m.

- Image of diaphragm when it's in the caudal position. It has to be chosen manually form the list of sequence images. Denoted as I_B.

- Contour of diaphragm in both caudal and cranial position. This is done by laying several points on a diaphragm contour. Amount of points is up to operator. More points lead to more accurate diaphragm localization and therefore more accurate results of computed parameters.

- Localization of all markers fixed on proband's body. Localization is done only on the first image of sequence.
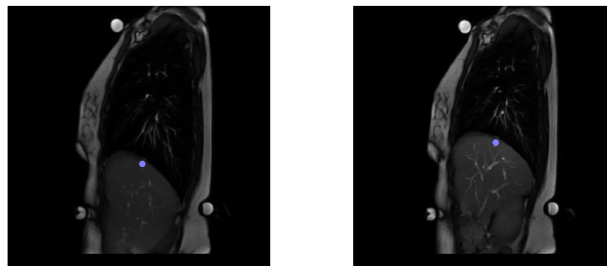
FIGURE 3.2: Point P_m and how it moves along with diaphragm contour.

Developed gui serves as environment for inserting these values, see sec 3.3.

Remaining values for parameters extraction are computed automatically, these are:

- Localization of point in every image of processed sequence.

- Loacalization of markers in all images of a sequence.

- Difference area a_t for every image resulting to breath-curve.

Above values serve for computation of all features which were introduced in the work (listed in sec. 4.1).

3.2.2 Breath-curve computation by image processing

Following algorithm is used for breath-curve computation:

1. First difference image Di_t for every image (t = 1 ... N, where N is number of images) is computed.

$$Di_t = I_t - I_B \tag{3.1}$$

   Where I_t denotes t-th image in sequence.
   Subtraction of images makes dark part of I_t which are still. As diaphragm moves bright crescent is produced in a diaphragm movement path. See upper left image in the figure 3.3.

2. Area of the crescent from previous step is our desired difference area a_t.

3. The crescent is detached from background by thresholding of Di_t (see upper right image in the figure 3.3). Thresholding evokes decomposition of Di_t onto distinct regions which can be easily labeled and further processed. Our goal now is to locate distinct region which represents a_t.
   Threshold value is computed from small area $(20 \times 20)px = I_{ar}$ around central point P_m as follows:

$$T = max(I_{ar}) \cdot T_c \tag{3.2}$$

   where T_c stands for constant defined for every image sequence manually to make a_t as much as close to diaphragm motion as is possible. T_c values are listed in tab. 3.1. Threshold value is computed for every image in the sequence apart.

4. Now the detection of desired labeled region has to be done. Before actual decision of which region is the searched one, restriction (denoted $R1$) on investigated

regions is assumed. We care only about regions in the image bordered by diaphragm's caudal and cranial contour proposed in the beginning of the section. All values in Di_t which are outside of this border are set as 0. See lower left image in the figure 3.3.

5. Desired region is now found by following equation:

$$a_t = max_i(-3 \cdot \frac{D_i}{256} + 25 \cdot \frac{S_i}{256^2}) \tag{3.3}$$

D_i denotes distance between i-th examined region and central point P_m, S_i denotes area of investigated region.

6. Once desired region is detected its area is stored as t-th value of a breath-curve.

Adaptive threshold computation eliminates trend of brightness changes. But fast isolated brightness changes can produce sudden changes a_t's area and thus add noise to computed breath-curve. To eliminate this exponential loss of threshold value is used. That means actual threshold value is computed according to following equation:

$$T_{ca}(t) = 0.3 \cdot T_c(t) + 0.7 \cdot T_{ca}(t-1) \tag{3.4}$$

$T_{ca}(t)$ denotes threshold value which is used for t-th image thresholding. $T_{ca}(t-1)$ denotes threshold from previous image. $T_c(t)$ denotes threshold computed from actual (t-th) image according to eq. 3.2.

3.3 Graphical user interface and its features

Graphical user interface was developed to provide control over image sequences. It serves as an image viewer, allows inserting above stated (3.2.1) input data, FFT spectrum processing for res- and pos- curve extraction and viewer for inspection of features' statistical properties. Main window of the interface is shown on fig. 3.4.

The panel titled **Main panel** shows both image I_t and difference image Di_t. Graph below main panel shows a breath-curve once it is estimated. In the left part of the interface lies images list, patient and measure selection. Above buttons serve for changing shown panel (Main panel, FFT processing panel, statistics panel) and for inserting input values described in 3.2.1. We will briefly describe features of every remaining panel.

FFT Analysis panel
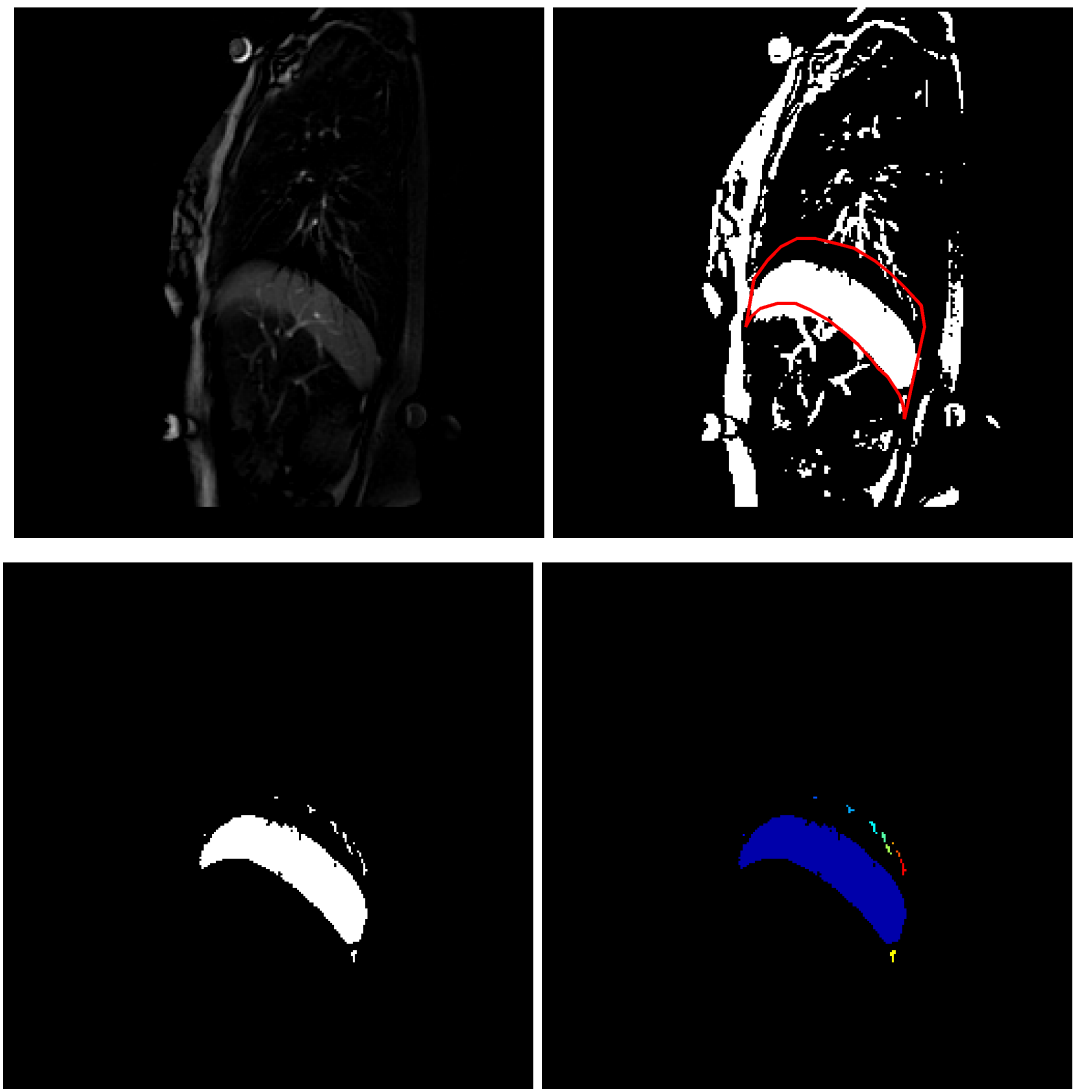
FIGURE 3.3: Images in this figure show steps for extraction of a region which belongs to a_t. Upper part of the figure, left to right: Di_t and thresholded Di_t. The lower part of the figure shows thresholded Di_t with restriction $R1$ applied. And on the right labeled distinct regions (every label is shown as a different color).

FFT analysis panel is shown if figure 3.5. In the main axes occurs FFT spectrum of signal shown in axes below it. Colored dots laid on the spectrum has their respective inverse curve shown also in the lower graph. Curves are in the same color as the dots. Operator chooses desired harmonics for inverse transform by clicking on the spectrum course. Technical aspects of pos- and res- curves extractions are discussed in following sections — 3.4.2 (curves properties analysis), 3.4.2.1 (its limitations). It is also possible to filter breath-curve with moving average filter filtering the frequency of breath due to get exact shape of pos-curve (see sec. 3.4.2.2).

Statistics panel

TABLE 3.1: This table shows values of threshold for processing image Di_t.

Healthy group				Pathological group			
Proband's number	S_A	S_B	S_C	Proband's number	S_A	S_B	S_C
1	0.45	0.40	0.20	17	0.15	0.10	0.10
2	0.45	0.50	0.20	18	0.23	0.15	0.10
3	0.30	0.30	0.20	19	0.15	0.23	0.10
4	0.20	0.40	0.30	20	0.23	0.23	0.10
5	0.30	0.30	0.20	21	0.05	0.10	0.10
6	0.30	0.30	0.20	22	0.20	0.20	0.10
7	0.30	0.30	0.20	23	0.10	0.10	0.10
8	0.20	0.25	0.30	24	0.15	0.05	0.05
9	0.30	0.30	0.20	25	0.20	0.25	0.05
10	0.30	0.20	0.20	26	0.15	0.10	0.05
11	0.30	0.30	0.20	27	0.15	0.05	0.05
12	0.20	0.40	0.10	28	0.10	0.15	0.05
13	0.30	0.30	0.10	29	0.10	0.10	0.05
14	0.30	0.40	0.30	30	0.15	0.15	0.05
15	0.20	0.30	0.30	31	0.25	0.10	0.05
16	0.40	0.40	0.30	32	0.10	0.10	0.05
				33	0.10	0.05	0.05
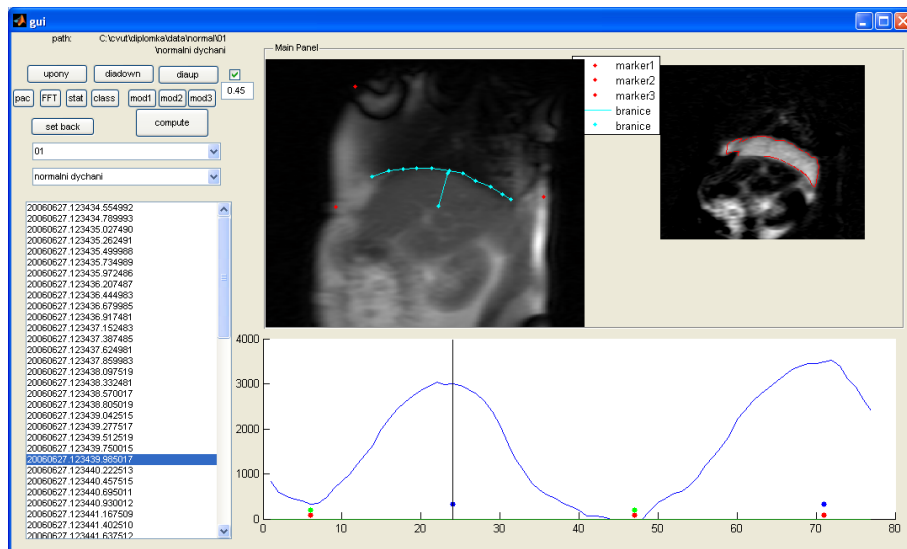
FIGURE 3.4: Illustration of the main window of graphical interface.
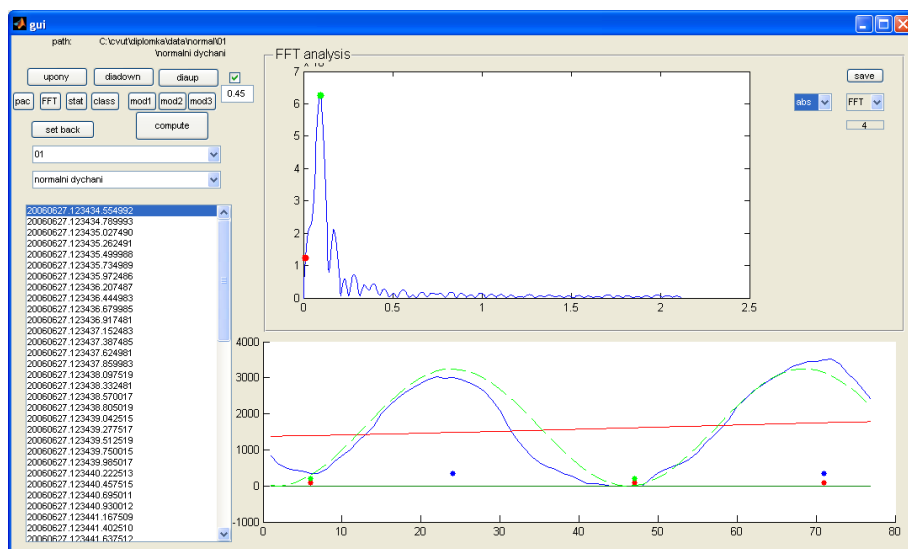
FIGURE 3.5: This panel serves for extracting pos- and res- curve from breath-curve.
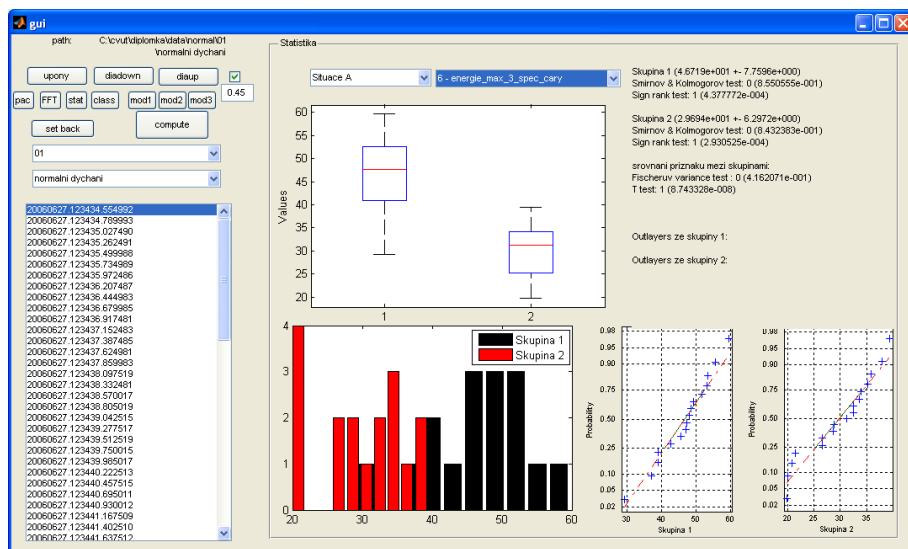
FIGURE 3.6: This panel serves for exploring statistical properties of extracted features.

Statistic panel is shown in figure 3.6. In its upper part are placed lists for patient and measure selection. Under them axes for box plot graphs are placed. On the right is place for statistical results (mean, std, KS test, Fisher test, T-test). In the lower part data histograms and normal probability plots occurs. Statistics serves for medical hypothesis testing. It shows whether there are statistically significant differences between proband groups.

3.4 Methods used for information extraction

3.4.1 Breath-curve processing

In breath-curve processing two main approaches were used. First method involves features gained from FFT spectrum of a breath-curve. Second approach uses the central statistical moments. As moments are well known and self explanatory we will discuss only physiological aspects of their usage in section 4.2.5 and focus on the first approach - FFT spectrum processing. It brought us some interesting revelations about diaphragm motion processing and physiological results. We will introduce and analyzed our application of this signal processing method in the following section.

3.4.2 Breath-curve FFT spectrum analysis

We used Fast Fourier transform for obtaining harmonics decomposition of a breath-curve. We don't describe Fourier transform here, but for further reading we recommend literature [10] or [11] or in english [12]. We mentioned earlier that breath-curve should be more or less harmonic when obtained from healthy breath sequence. We suppose occurrence of one distinct peak in harmonic spectrum of the breath-curve. In figure 3.7 example of typical breath-curve (upper image) and its corresponding spectrum is shown.

One main frequency of breath is significant in the upper part of fig. 3.7 though depth of breath wasn't steady through the sequence. When we look at the lower image in fig. 3.7 we see that the spectrum contain one great peak on a frequency of approximately 0.4 Hz. This peak relates to breath frequency. But it is not the only significant peak in this spectrum. There is a second one carrying harmonic with frequency 0.03 Hz. This harmonic relates to breath depth changes. It is clearly visible on next figure 3.8 where harmonic components on selected frequencies were restored by inverse FFT.

We named above construed curves as follows:

- The curve corresponding to breath frequency originates from diaphragms respiratory function. We called it `respiratory curve` or simply `res-curve`.

- Other curve principally situated on lower frequency originates from diaphragm postural function (or disfunction) thus we call it `postural curve` or `pos-curve`. Often we talk about average diapgragm position. By this we mean average through breath period ($\frac{1}{breath frquency}$).
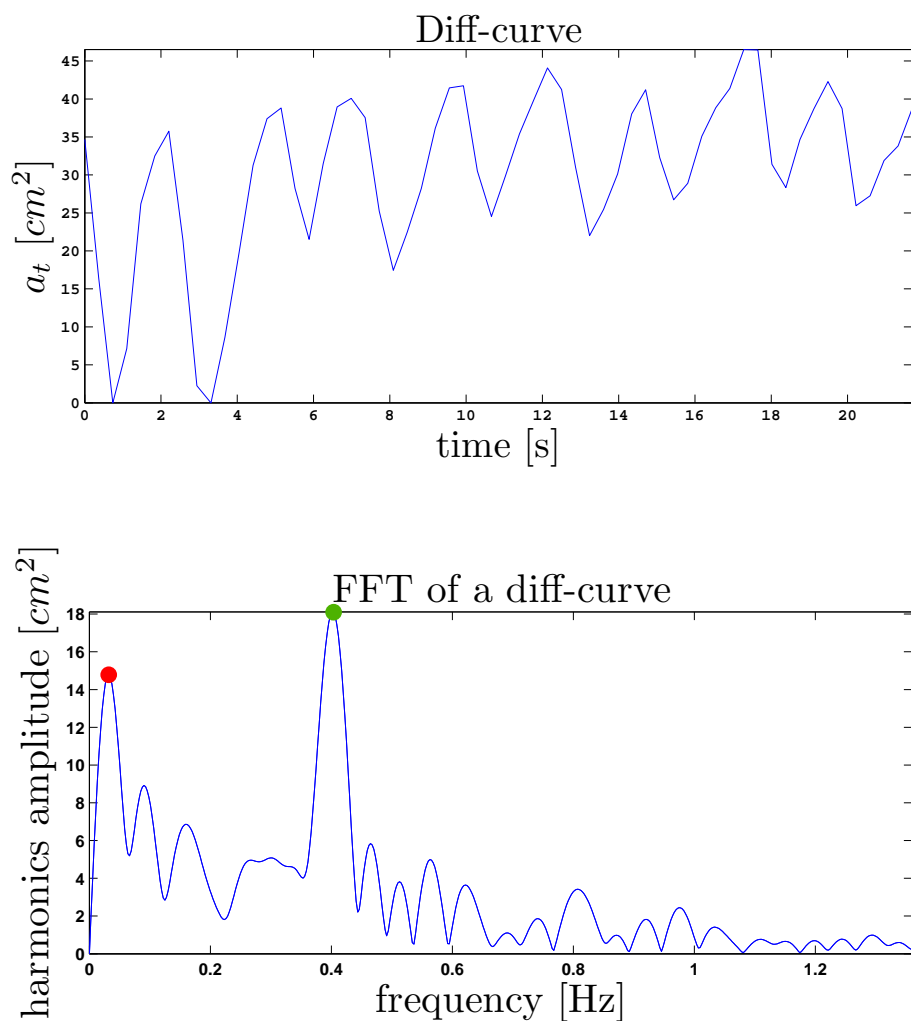
FIGURE 3.7: This figure shows a diff-curve and its corresponding FFT spectrum. There are two significant peaks everyone corresponding to one diaphragm function. Their description follows under the figure.

- Green point lies on a peak corresponding to respiration part of diaphragm movement. Its restoration by inverse FFT can be found on next figure (3.8). We called it **res-curve**.

- Red point lies on a peak related with diaphragm average position changes, i.e. diaphragm postural function. Restoration of this curve can be also found on figure (3.8). Curve was called **pos-curve**.
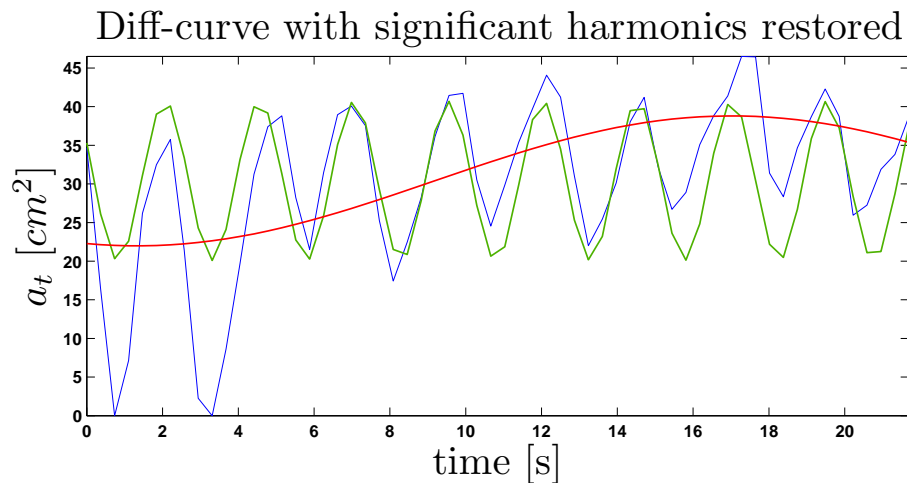
FIGURE 3.8: This figure shows restored significant harmonics from FFT spectrum of a breath-curve. Pos-curve is plotted red and res-curve is plotted green.

3.4.2.1 Res- and pos-curve extraction limitations

Although res- and pos-curve extraction works very well for harmonic breath with slow average diaphragm position changes, there are few important limitations which should be kept in mind while using our proposed method. In section 5.1.1 we suggest some solutions when below described problems occur.

▷ **Breath frequency changes within measured sequence.**

Breath frequency isn't constant during breathing. Even for 20 s long sequences used by us there were frequency drifts. Situation is illustrated by figure 3.9. There is shown breath-curve with frequency fluctuation and its corresponding FFT spectrum. It is visible that restored harmonic from spectrum follows original breath-curve only in parts of its course. In lower part of the figure mean of the two curves is shown. The last curve evidently follows original curve more precisely.

When this limitation occurs in a sequence then harmonic with biggest correlation (as FFT rates individual harmonics by correlation) with breath-curve must be chosen. As the sequences aren't long, no big fluctuation of breath frequency occurs. Also it is up to operator to select and to rate quality of restored curves whether pos- or res- curves characteristics should be used as features or removed from observed set due to method incompetency.

▷ **Breath isn't harmonic.**

Sometimes breath-curve doesn't have harmonic shape. It occurs mostly when
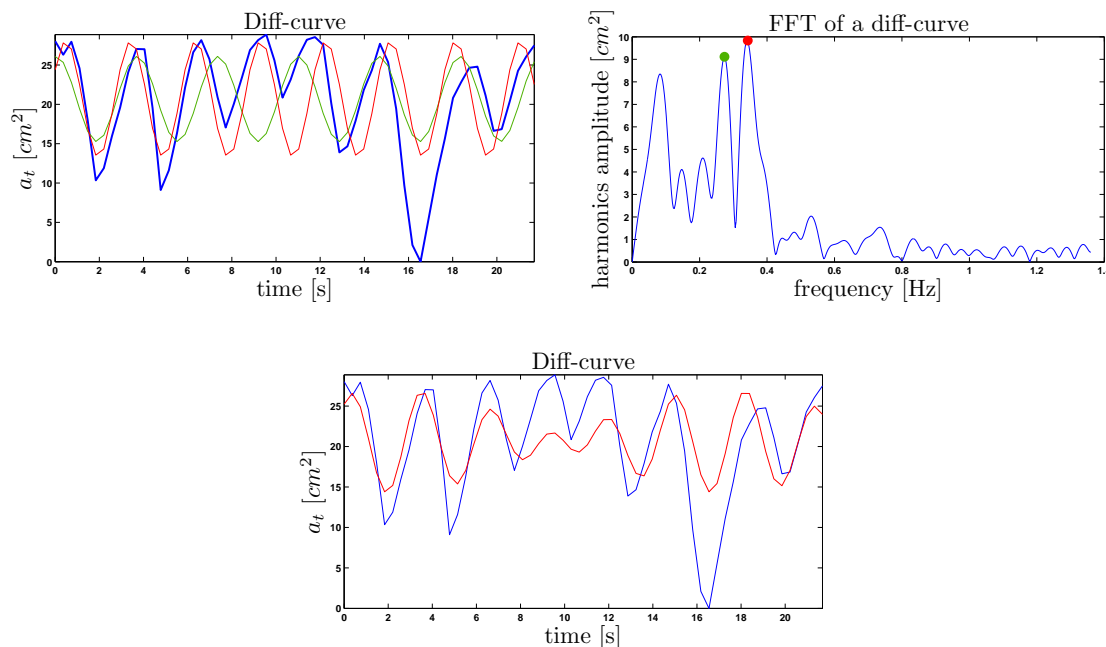
FIGURE 3.9: This figure illustrates how frequency fluctuation during breathing change spectrum shape. Now two peaks corresponding to respiration curve occur. Upper images shows breath-curve with restored selected harmonics on the left. And on the right it shows spectrum of breath curve with highlighted points to restore. Lower part of figure shows mean of the two restored curves.

diaphragm has to ensure postural function. In our case this problem occurred sometimes when proband had to deal with pressure on lower limbs. It is possible that only pos-curve can be extracted from breath-curve as it doesn't do any harmonic motion and only change its average position. Example of breath like this with its corresponding spectrum is on figure 3.10. The figure shows breath-curve and also average restoration of two most significant spectral peaks (see figs 3.10 description for details) colored red. We can see it follows trend of the breath-curve and could use amplitude of a curve, but it wouldn't be much accurate. Then for approximation by only one curve (as proposed for this method) we can't get enough accurate results.

▷ **Limitaions of pos-curve aproximative character.**
  The last notice deals with the pos-curves approximative character. In a case of pos-curve it should be kept in mind that we use harmonic function as approximation of diaphragm average position changes. Amplitude of this approximation is good parameter to show how large drift diaphragm performed during breathing. We would like to express speed of this change too. We proposed to use frequency of a pos-curve resulting in selection of the harmonic frequency. Problem is that real pos-curve doesn't tend to be
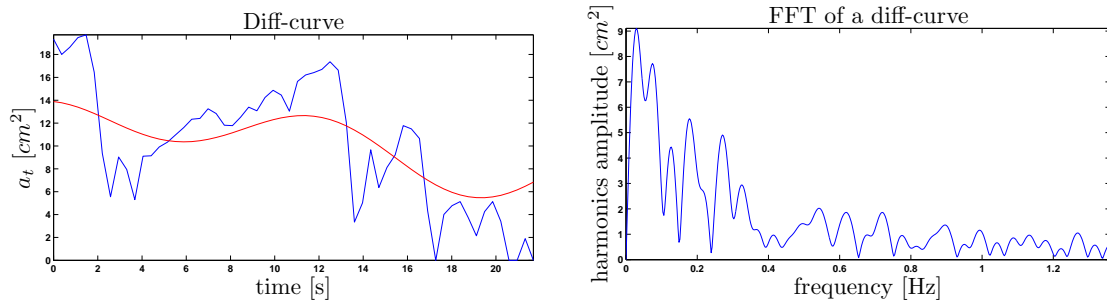
FIGURE 3.10: Figure shows breath curve that is not harmonic (on the left). Red curve is average of two restored peaks in spectrum which are most significant. Spectrum itself is shown on the right (the peaks are those on the left part of spectrum).

harmonic-like function like a respiration is. Thus its frequency has not any real meaning. It shows roughly how fast diaphragm's average position drifted but spread to the whole sequence duration. Image in figure 3.10 express what we tried to point out in this paragraph.

3.4.2.2 Real shape of pos-curve extracted by filtering breath-curve with moving average filter.

We stated that harmonic approximation of pos-curve isn't very satisfactory for many breath courses. One approach how to extract real breath curve when breath is harmonic is to filter the breath-curve with moving average filter with length corresponding to breath period. When we filter the frequency of breath away with low-pass filter we obtain curve corresponding to average diaphragm position drift during breathing. Example is shown in figure 3.11.

We can see on figure 3.11 that breath-curve filtered with simple moving average filter follows more precisely the average position of the breath-curve. Problem is that for proper shape of pos-curve mustn't frequency of the breath-curve change during breathing. Also this simple filtration shorten output pos-curve by filter length. It means that the slower breath is the shorter resulting pos-curve would be. Also the real curve is hard to objectify. More parameters would be necessary for describing shape of this curve but interesting physiological results could be obtained if done so. Adaptive filtration of a breath curve or more sophisticated parametrization of this method obtained pos-curve could be interesting course of future work direction.
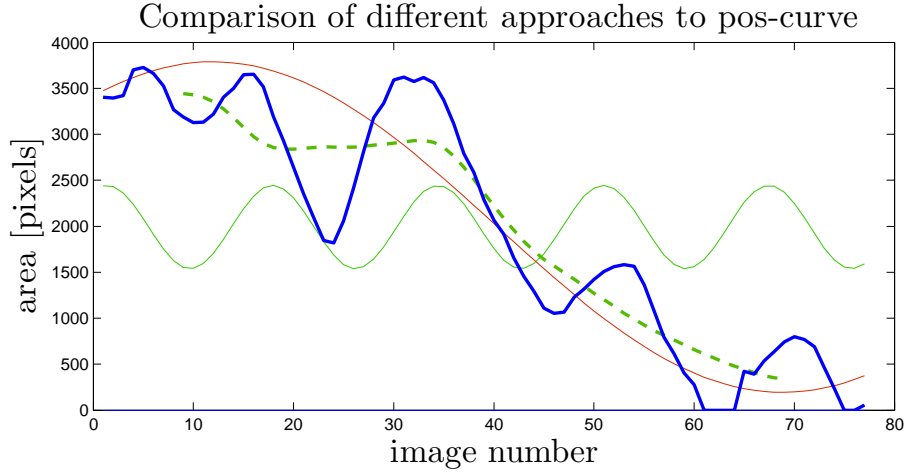
FIGURE 3.11: This picture shows pos-curve obtained by filtration of breath-curve with moving average filter with length respective to res-curve frequency. By filtration obtained curve is the green dashed curve, bold blue curve is the breath-curve.

3.4.3 Fitting into diaphragm

For diaphragm shape assessment we used different shapes fitted into diaphragm contour. Features dec_a, dec_r, ρ_d, e_d from section 4.1 are based on fiting of a line, circle or ellipse into diaphragm contour. In this section we describe methods used for fitting.

3.4.3.1 Linear regression

For diaphragm declination comparison between observed groups we need to guide a line through its contour. This purpose was done by linear regression of contour data. To aim this, classical least squares method was used. As source data for fitting aren't fundamentally linear we don't use linear regression in classical way. Our goal is to objectify diaphragms shape and express its declination. Thus we don't use any methods for outlayer suppression.

Main aim of least squares method is as follows:

Consider equation of a line:

$$y = p_1 \cdot x + p_2 \tag{3.5}$$

Then subsequent system of n linear equations is created:

$$S = \sum_{i=1}^{n} [y_i - (p_1 \cdot x + p_2)]^2 \tag{3.6}$$

n is length of input data; when is longer then 2 then system is overdetermined (and result is the best solution under the constraint of minimizing S). x_i, y_i stands for the diaphragm data and p_1 and p_2 are line parameters.

Equation (3.6) expresses sum of squares of residuals (difference between fitted values and desired ones, for us it is $[y_i - (p_1 \cdot x + p_2)]$). Aim of least squares method is to minimize S.

For realization we used function `robustfit` from Matlab Statistics toolbox for solving system of equations (3.6). As an input parameter we set up *'ols'* which stands for ordinary least squares method. Example of fitted line for patient group C_1 and C_2 follows.
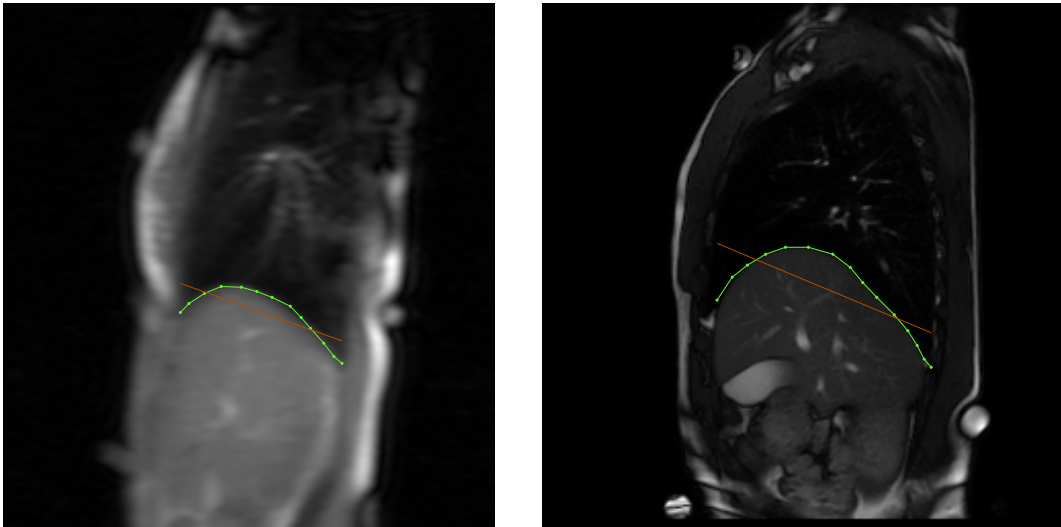
FIGURE 3.12: Example of line fitted into diaphragm contour for both proband groups.

3.4.3.2 Circle fitting

Circle fitting can be done directly from above described linear regression by substituting parameters in equations.

Consider equation of a circle as follows:

$$
\begin{aligned}
(x - m)^2 - (y - n)^2 &= r^2 \\
-2mx - 2ny + m^2 + n^2 - r^2 &= -x^2 - y^2
\end{aligned}
\tag{3.7}
$$

Now we use following linear system equation written in matrix form:

$$\begin{bmatrix} 1 & x_1 & y_1 \\ & \vdots & \\ 1 & x_n & y_n \end{bmatrix} \cdot \begin{bmatrix} p1 \\ p2 \\ p3 \end{bmatrix} = \begin{bmatrix} -x_1^2 - y_1^2 \\ \vdots \\ -x_n^2 - y_n^2 \end{bmatrix} \tag{3.8}$$

where $x_1 \dots n$ and $y_1 \dots n$ stands for diaphragm contour data. Equation system processing is similar to fitting a line in previous section. And the minimization constraint becomes:

$$S = \sum_{i=1}^{n} [-x_i^2 - y_i^2 - (p_1 + p_2 \cdot x_i + p_3 \cdot y_i)]^2 \tag{3.9}$$

where i ranges through data length $1 \dots n$.

As substitution for circle fit was used, after solving equation system (3.8), (3.9), desired parameters are as follows:

$$
\begin{aligned}
p_1 &= m^2 + n^2 - r^2 \\
p_2 &= -2m \\
p_3 &= -2n
\end{aligned}
$$

Circle parameters are then:

$$
\begin{aligned}
r &= \sqrt{m^2 + n^2} \text{ for diameter} \\
m &= \frac{-p_2}{2} \text{ for x-axis shift} \\
n &= \frac{-p_3}{2} \text{ for y-axis shift}
\end{aligned}
$$

Matlab function `robustfit` with apropriate input (ordinary least squares method and diaphragm contour data) was used for actual fitting. Example of circles fitted into random probands from both proband groups follows on figure 3.13.

3.4.3.3 Ellipse fitting

Ellipse fitting was done also by least squares minimization. As ellipse fitting method is more complex we used stable robust method proposed by [13]. This method is based on using generalized eigenvectors of matrices.
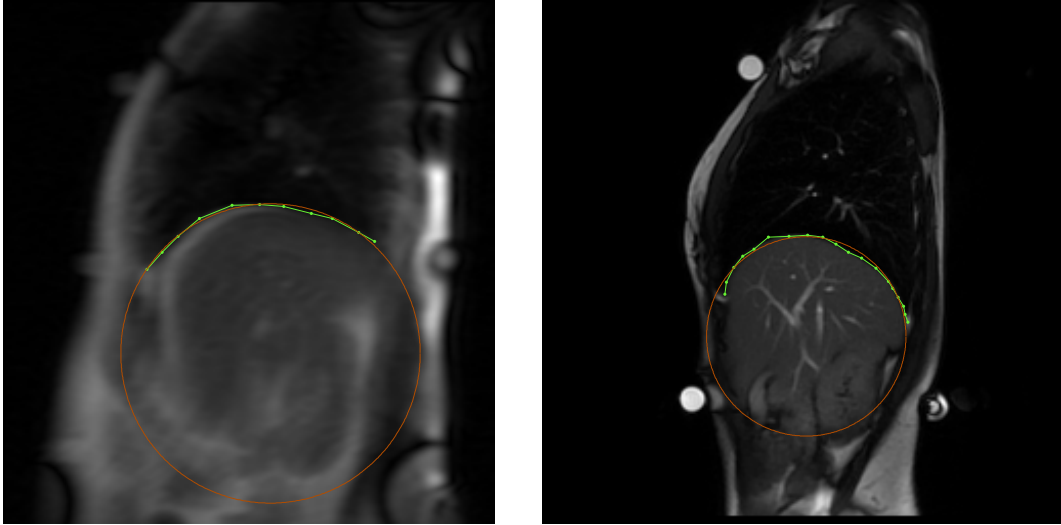
FIGURE 3.13: Example of circle fitted into diaphragm contour for both proband groups.

An ellipse equation is as follows:

$$F(x, y) = ax^2 + bxy + cy^2 + dx + ey + f = 0 \tag{3.10}$$

with constraint

$$b^2 - 4ac < 0 \tag{3.11}$$

$a, b, c, d, e, f \in \mathbb{R}$ are coefficients of an ellipse. $F(x, y)$ is algebraic distance of point (x, y) from the ellipse. In [13] authors then define:

$$\vec{a} = (a, b, c, d, e, f)^T$$
$$\vec{x} = (x^2, xy, y^2, x, y, 1)$$

it is possible to rewrite equation to matrix representation

$$F_a(\vec{x}) = \vec{x}\vec{a} = 0 \tag{3.12}$$

Fitting into data set $(x_i, y_i), i = 1..N$ is then characterized by this minimization constraint:

$$min_a \sum_{i=1}^{N} F(x_i, y_i)^2 = min_a \sum_{i=1}^{N} (\vec{x_i} \cdot \vec{a})^2 \tag{3.13}$$

Constraint (3.11) must be kept in mind to get an ellipse as a result. Authors then deals with computation stability and fitting quality which is ideal for our purpose. Example of fitted ellipse for both proband groups follows on figure 3.14.
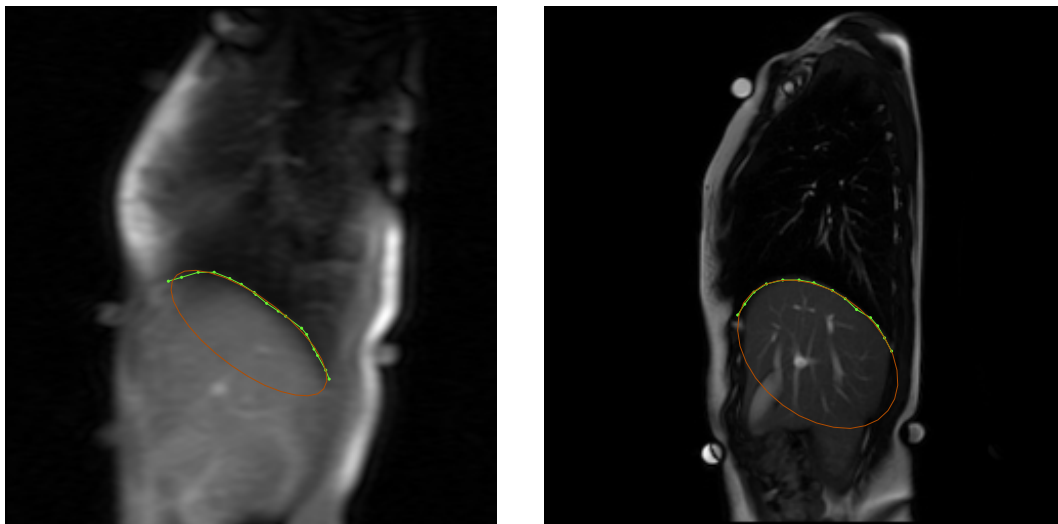
FIGURE 3.14: Example of ellipse fitted into diaphragm contour for both proband groups.

3.4.4 Statistics

Source of information for following procedures was [14]. For inter group differences evaluation simple t-test was used. Procedure used for test was following:

1. **Test for verification of dataset normal distribution.** Single sample Kolmogorov-Smirnov test was used to proof whether variable values come from normal distribution. Normal distribution tested against our variable was produced by estimation of mean and var of the processed variable. Then normal distribution with respective mean and var parametrs was used as input for function `kstest` performing this test in Matlab.

2. **Test for inter-set variation unity.** Two-sample F test for equal variances was used to perform this test. Two compared datasets were used as an input for this test and whether equality or unequality of datasets variances was passed to Students T-test in next section. Matlab function `vartest2` performed this testing.

3. **Test for unity of mean values of datasets.** Classical Students T-test was used to perform this test. If condition of normal distribution in step 1 was fulfilled then by Matlab function `ttest2` with respective variance similarity estimation from step 2 was called.

Statistical test was performed on significance level of 0.05 of 0.001. See results section for details 5.2.

3.4.4.1 Outlayers treatment

In every statistical testing first possible outlayer data were removed from set. Value was marked as outlayer when its value was out of defined range:

$$\text{proper data range } = \langle 25\% \text{ quantil} - w \cdot iqr(X), 75\% \text{ quantil} + w \cdot iqr(X) \rangle \qquad (3.14)$$

where *iqr* stands for 75 % and 25 % quantil difference.

X stands for observed values set.

w is a constant defaultly set to 1.5.

Chapter 4

Features

4.1   What we extracted

For consecutive medical work numerous features were extracted from available breath sequences. The features can be basically divided into 2 groups.

- Dynamic features

- Static features

Dynamic features deal with diaphragm movement while static features observe diaphragm position, declination, overall profile and shapes changes during breathing and through situations.

Static features could be extracted from all observed situations - A, B, C. Dynamic features inasmuch as deal with motion could be extracted only from situations A and B.

List of both dynamic and static features with descriptions:

Dynamic features:

- Frequency and amplitude of res-curve: $f_r[Hz]$, resp $a_r[-]$.

- Frequency and amplitude of pos-curve: $f_p[Hz]$, resp. $a_p[-]$. If diaphragm excursion is strictly symmetric, than $f_p = 0$.

- Amplitudes ratio of res- and pos-curve: $r_{rs} = \frac{a_r}{a_s}$.

- The percentage of energy yielded by the three biggest spectrum lines: $p_3[\%]$.

- Standard deviation, skewness and kurtosis of breath curve: $\sigma_{DC}, \gamma_{DC}, \beta_{DC}$.

Static features:

- Diaphragm declination in sagittal plane in both caudal and cranial position: $dec_a[°]$, resp. $dec_r[°]$

- Partial height of a diaphragm in 5 different points equally placed on a diaphragm $b_i; i = 1, .., 5[-]$.Diphragm height is measured in it's lowest position (during full breathe in).

- Vertical distance from point b_5 and back marker (syrenge): $vd_6[-]$. This parameter correspond to diaphragm height in thorax.

- Relative position of the highest point lying on a diaphragm contour between diaphragm margins: $c_d[-]$.

- Sagittal size of a thorax: $t_s[mm]$.

- Height of a strip overlapping diaphragm contour parallel to line fitted to the contour: $h_d[-]$.

- Diameter of a circle fitted to a diaphragm contour: $\rho_d[-]$.

- Eccentricity of an ellipse fitted to a diaphragm contour: $e_d[-]$.

- Angle between a line fitted to the diaphragm contour and horizontal line: $\delta[°]$.

- Angle between a secant guided through highest point on a contour and a point lying on a contour 2 centimeters forward horizontal line, resp. 6 centimeters backward horizontal line: $\alpha_2[°]$, resp. $\alpha_6[°]$.

As you can see every feature which describes distance except saggital thorax width are dimensionless. These features - $b_1..b_5$, h_d, ρ_d - were always normalized by diaphragm countour marginal points distance (saggital thorax width - t_s) and a_r, a_p are normalized by square of t_s. It was done due to remove dependency of these features on patient's sagittal thorax width which we assumed.

4.2 Dynamic features

4.2.1 Frequency and amplitude of res-curve: f_r, a_r.

Methodology of this feature if proposed in section 3.4.2.

When spectral analysis of res-curve is processed, frequency and amplitude of harmonic carrying the biggest amount of energy are used as a features (see figure 3.1). Due to breath's very harmonic course, we can measure it's frequency. If breath frequency changes through observed cycle, only one has to be choosed (see sections 3.4.2.1, 5.1.1 for discussion). Nevertheless sometimes - and mainly when some activity during breathing is practised (like in situation B - pressure against lower limbs) - breath could be non-harmonic. It can be more like held breath or pulse or step function (see image 3.10). Regardless FFT transform can still be processed and harmonic with biggest amount of energy can be estimated. But this would lead to misinterpreted meaning of this parameter, so f_r, a_r should be removed from observation set when this situation happens. Also no automatic algorithm was made to decide whether to remove measure or not, so breath curve has to be watched manually.

4.2.2   Frequency and amplitude of pos-curve: f_p, resp. a_p.

Methodology of this feature if proposed in section 3.4.2.

By measuring frequency resp. amplitude of a pos-curve we tend to obtain features describing changes in average diaphragm motion. Ideal diaphragm motion while breathing is believed to be harmonic and thus symmetrical around average position. We hypothesize that bigger changes in average position prove worse stabilization and postural abilities of the diaphragm. Thus breath curve is fitted with harmonic function found by processing its spectrum obtained by FFT, we try to find some peak low frequencies area which corresponds to this proposed average diaphragm position movement. If there isn't any peak visible we tried to find some point which gave us a visibly corresponding curve after inverse Fourier transform. Both f_p and a_p equal 0 in the best case of ideal breath.

4.2.3   Amplitudes ratio of res- and pos-curve: r_{rs}.

Problem occurred while studying a_p's properties. It is that a_p is actually function of breath amplitude. What we want to evaluate is how big part of breath amplitude pos-curve takes. To obtain this new feature was introduced as a a_r and a_s ratio.

4.2.4   The percentage of energy yielded by the three highest spectrum lines: p_3.

To estimate how harmonic the breath is, we measure amount of energy yielded by 3 largest harmonics in a FFT spectrum of breath curve. We suppose that when the breath

is more sinus-like larger amount of energy will be carried by these 3 harmonics. 128 point FFT spectrum was used as basis of this feature, although only first half of spectrum was used due to Fourier spectrum symmetry, feature was calculated from 65-point spectrum.

4.2.5 Standard deviation, skewness and kurtosis of breath curve: σ_{DC}, γ_{DC}, β_{DC}.

Second, third and fourth central statistical moments are used directly as features in our work. Easy implementation and interesting physiological contexts make central moments good for using as a features. We suppose that central statistical moments are well known, so we don't need to introduce them here. For everyone interested we used following literature as reference [14].

Standard deviation expresses height of breath curve - how deep breath actually is. Because it characterize height of breath-curve i.e. height of a diaphragm movement. Results can be found in 5.2.

Skewness expresses how centered values are in probability distribution of subject variable. It means we observe non-zero skewness when marginal values from one side of its range occur more often then values from the other side. For physiological interpretation that means we get positive resp. negative skewness if breath curve is not symmetric i.e. we get positive skewness when proband tended to keep diaphragm in breathe-in for longer time than breathe-out and vice versa.

Kurtosis expresses how much pointy the probability distribution is. Again, sinus has very low kurtosis. When proband tend to loose control over diaphragm motion kurtosis is believed to rise, because values distribution of a breath curve reshape closer to normal distribution as values of the curve become more random. Kurtosis also deals with our problem with some special cases of FFT analysis (sec. 4.2.1 and 4.2.4). Then kurtosis or better the whole vector (σ_{DC}, γ_{DC}, β_{DC}) can be used as a main resulting feature for deciding of proband diaphragm control.

4.3 Static features

4.3.1 Diaphragm declination in sagittal plane in both caudal and cranial position: dec_a, resp. dec_r

Diaphragm declination is an angle between horizontal line and a line fitted into diaphragm contour (see fig. 4.1) in both caudal and cranial position. Line is fitted by

robust linear regression using least squares as a core method (see section 3.4.3.1 for details). Main goal is to compare diaphragm declination only, but feature summarizes diaphragm overall shape also and project it into declination (changes of shape also affect this feature). But as long as diaphragm is not rigid organ changes of it's shape should be taken into account in measuring its declination.
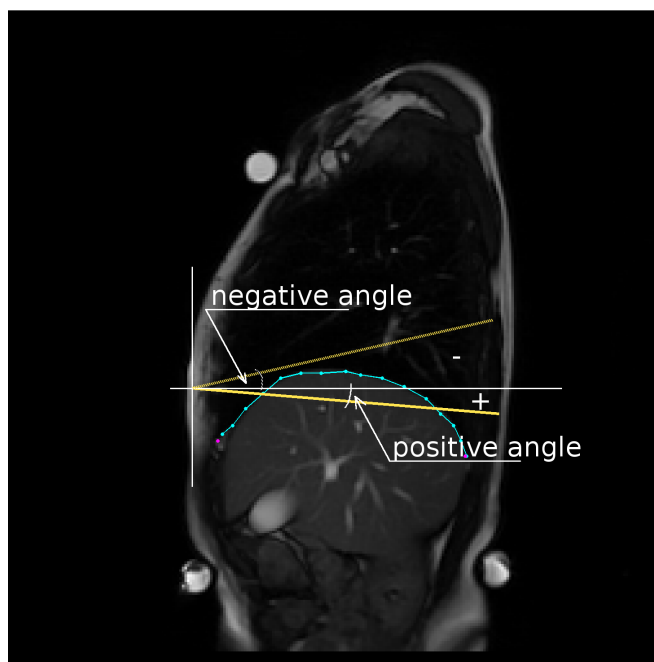
FIGURE 4.1: The thick yellow line is the one fitted to imaged diaphragm contour (blue dotted line). Its measured declination would be positive angle. If some other fitted line would be rotated as a dashed yellow line then the declination would be measured as negative.

4.3.2   Partial height of a diaphragm in 5 different points equally placed on a diaphragm $b_i; i = 1, .., 5$. Diaphragm height is measured in its lowest position (during full breathe in).

We measure this feature to realize if different parts of diaphragm differ in height between observed groups. By analyzing this feature between particular situations we can also determine changes in diaphragm shape within different situations. Feature was measured during full breathe-in ergo in lowest position. Situation is shown on fig 4.2.
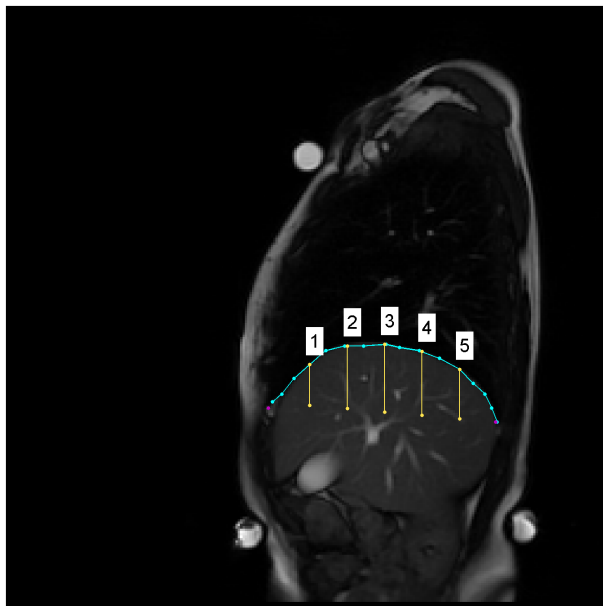
FIGURE 4.2: On this image division of diaphragm into 6 equal parts producing 5 points where diaphragm partial height is observed.

4.3.3 Vertical distance from point b_5 and back marker (synerge): vd_6, this parameter correspond to diaphragm height in thorax.

Fully self-explanatory title. We want to obtain and compare diaphragm height in thorax by this feature. Sign of vd_6 related to position around back marker shows figure 4.3. Big difference and hard verification of back marker position between two observed groups lower confidence in this feature. Feature was also removed while examining classification performance of data (sec. 6). As feature itself isn't completely confident, dependency on back marker position can be removed by computing difference between the feature in different measured situations.

4.3.4 Relative position of the highest point lying on a diaphragm contour between diaphragm margins: c_d.

Clearly explained by figure 4.4. Also this feature was introduced mainly to observe movement of this highest point through situations.

4.3.5 Sagittal size of a thorax: t_s.

Used for removing potential dependency of extracted features on probands width. Actually during some tests no such dependency occurred so normalization seems not to be necessary but for assurance was pursued anyway.
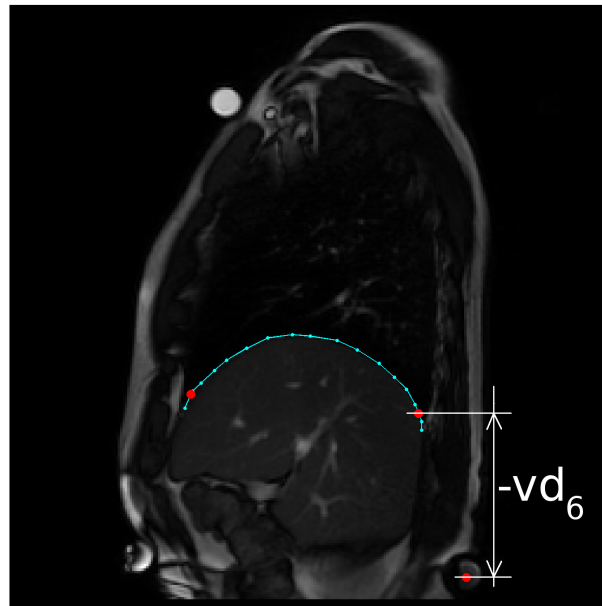
FIGURE 4.3: Figure shows sign convention for measuring vd_6. It was decided to put negative sign when diaphragm lies above the back marker.
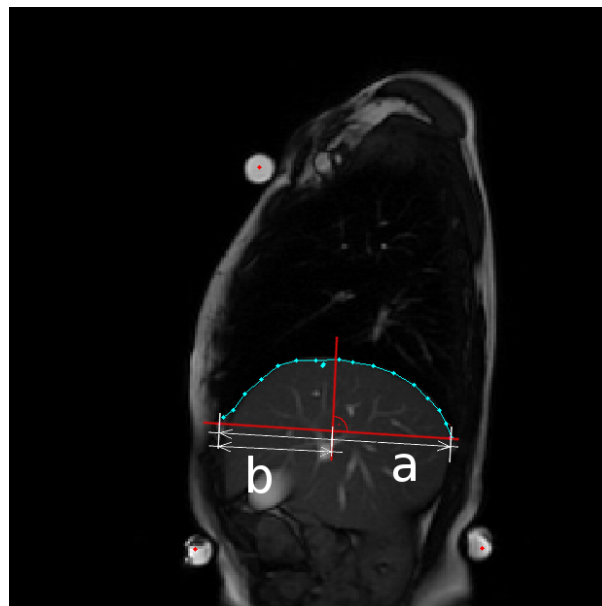
FIGURE 4.4: Here an explanation of a computation of relative position of the highest peak on diaphragm is demonstrated. $c_d = \frac{b}{a}$

4.3.6   Height of a strip overlapping diaphragm contour parallel to line fitted to the contour: h_d.

Height of diaphragm regardless of its declination was required to be measured so this feature was introduced. It uses line fitted through diaphragms contour (introduced in section 4.3.1) as a parallel line with the overlapped strip. Again we observed feature itself and also differences of strips height between situations. Details of measurement are easily explained in figure 4.5.
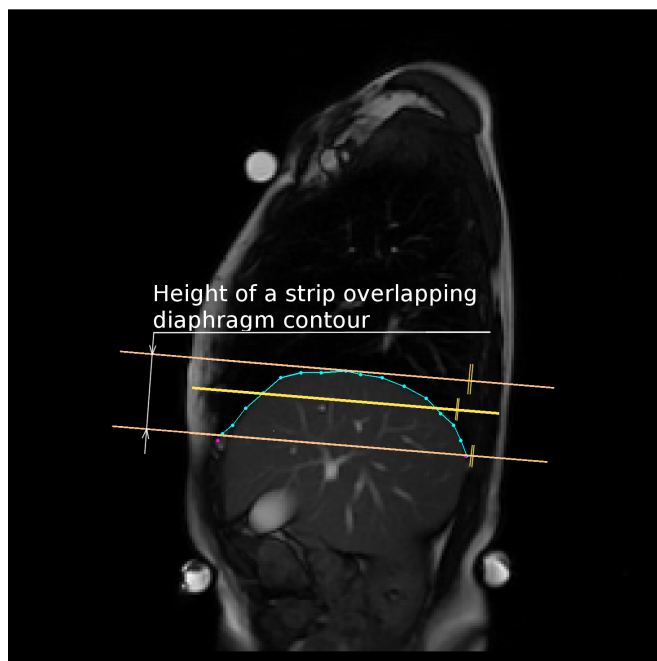
FIGURE 4.5: Blue line with dots is a diaphragm contour. Yellow line is least squares fitted line. And orange lines are margins of desired strip. It's apparent that strip is parallel to yellow line.

4.3.7   Diameter of a circle fitted to a diaphragm contour: ρ_d and eccentricity of an ellipse fitted to a diaphragm contour: $e_d[-]$.

Both features were introduced to describe flatness of diaphragm and differences of it between measured situations. Diaphragm seems more ellipse shaped but on the other hand circle diameter is more clear and simple parameter. Also for different probands ellipse can be fitted in different ways and therefore its eccentricity can describe different shape qualities. See fig. 4.6 for explanation. We will discuss differences between ρ_d and e_d in results section (5.2).
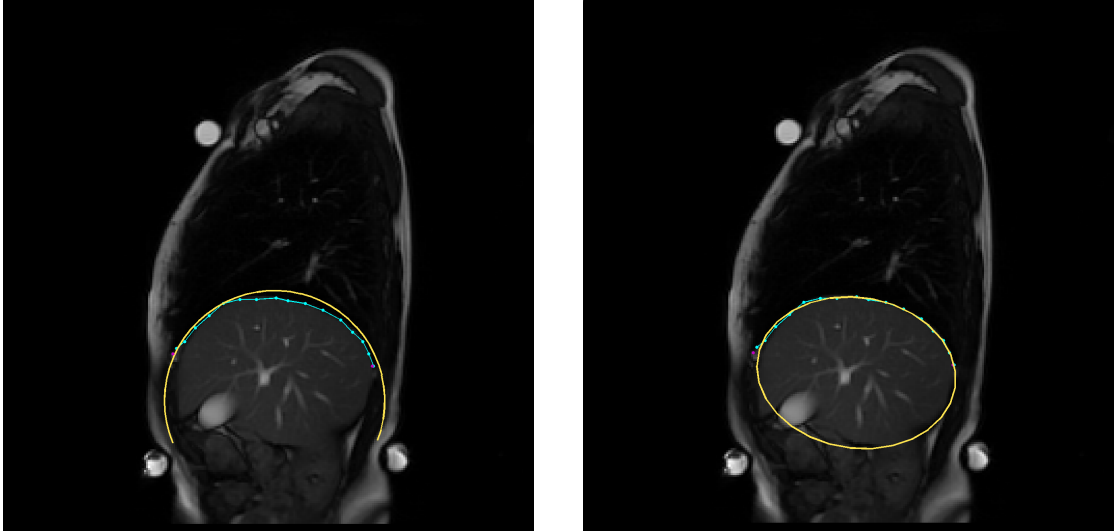
FIGURE 4.6: On left image a fitted circle is shown and on right image there is an ellipse fitted to the diaphragm contour. It's clear that ellipse fitts better to the contour of a diaphragm. This become even more obvious when diaphragm become flatter. More detailed outlook of advances and disadvantages is discussed in section 5.1.2.

4.3.8 Angle between a secant guided through highest point on a contour and a point lying on a contour 2 centimeters forward horizontal line, resp. 6 centimeters backward horizontal line: α_2, resp. α_6.

For observing declination frontal and rear part of diaphragm separately we divided it into two parts and measured two different angles as shown on image 4.7. With this feature we mainly focused on inter-situation differences between features. So we can determine how subject parts of diaphragm react on strain changes.
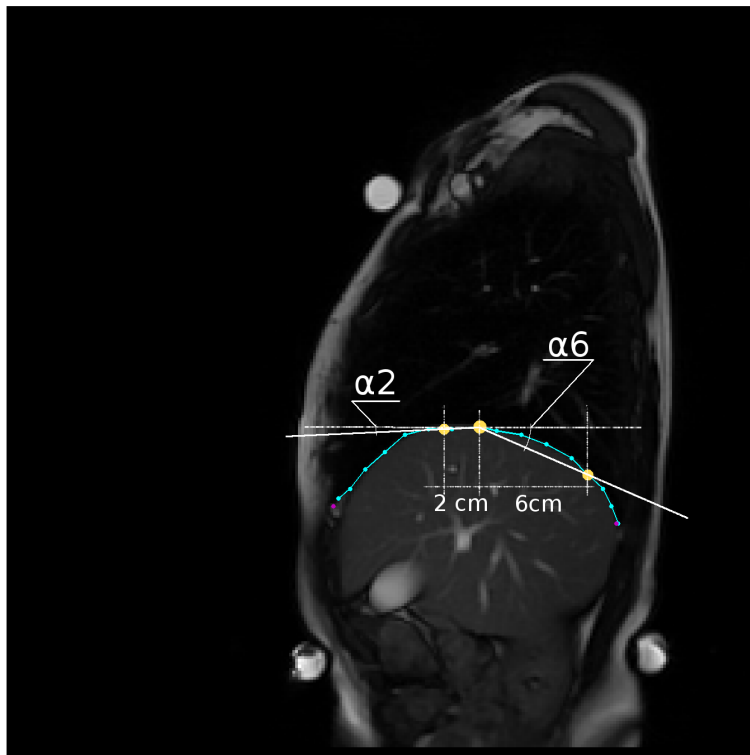
FIGURE 4.7: Figure which shows how angles α_2, resp. α_6 are measured.

Chapter 5

Feature limitations & statistical results

5.1 Feature limitations

Here we will discuss limitations of features presented in the previous sections. Most of the limitations was mentioned or discussed in other sections. We will summarize and bring detailed view on them here.

5.1.1 Limitation of breath-curve processing.

We proposed method for breath-curve assessment by processing its FFT spectrum. As was mentioned in the respective section 3.4.2.1 necessary condition for breat-curve assessment is that breath-curve has sinus-like shape.

If breath isn't harmonic, it means that proband can't handle diaphragm function properly and harmonicity (measure of harmonic shape similarity) of a breath-curve may be the first evaluative parameter of breath. For this purpose parameter p_3 can be used. This feature rates shape of breath-curve and objectify quality of its course in sense of harmonicity. Along with parameter p_3 further 4. central statistical moment (β_{DC}) rates breath-curve in parallel way. Parameter p_3 has its limitation for constant course of a breath-curve. It was discussed in section 4.2.5. It is that p_3 has the same value for constant breath-curve as for ideal harmonic breath (p_3 has higher values) and thus hold breath and harmonic breath aren't distinguishable. Parameter β_{DC} has large value for constant course of a breath curve and small value for harmonic course. Accordingly using both features for breath objectification gives good objectification tool for rating

41

basic quality of a breath course. Some problems could occur though. Section 5.2.1 suggests where eventual focus should direct.

Next limitation of the proposed method of breath-curve processing is mentioned inability to handle fluctuation of breath frequency during breathing. Section 3.4.2.1 deals with this problem. One single frequency has to be selected and used as a parameter characterizing breath-curve. We suppose that the selected frequency should be the one which leads to worse estimation of breath quality. Then if needed significant frequencies range could be added as parameter. Or future work could focus on breath-curve spectrogram processing. It could help for proper objectification of frequency changes during breathing.

5.1.2 Circle/ellipse fitting limitations.

Problem with fitting a circle into diaphragm contour is in variability of diaphragm shapes. Circle is exactly defined shape which we fit into diaphragm contour by minimization of square distances sum. Measuring of circle radius is done in order to extract its flatness. As diaphragm has complex shape circle doesn't fit in well every time and large amount of noise could occurs in results due to this inaccuracy.

Problem with ellipse fitting is similar. Due to fitted ellipse rotation the best fit always has different rotation and different part of an ellipse lies on a diaphragm contour. It can lead eccentricity to acquire inverse values than expected. This problem is illustrated on following images. More tests with ellipse fitting should be done with different restrictions on ellipse to find satisfactory result.

5.2 Results - statistics & observations

We present the most important statistical results of inter-groups features comparison.

5.2.1 Breath harmonicity

In previous section we estimated p_3 and β_{DC} as the best parameters for rating harmonicity of a breath curve. Measured results of these parameters are following:

In result there is significant difference between healthy group (C_1) and painful group. Values are as were hypothesized: group C_1 carries larger amount of energy according to parameter p_3. It is twice as much and for both situations it is very significant as seen above. For pathological group amount of energy decreases slightly more though

TABLE 5.1: Statistical Analysis of C_1 and C_2 for breath curve harmonicity.

	Feature	C_1	C_2	p-value
S_A	p_3	46.719 ± 7.760	29.694 ± 6.297	8.74e-008
S_A	β_{DC}	1.924 ± 0.394	2.233 ± 0.327	0.029
S_B	p_3	45.924 ± 5.322	25.035 ± 5.963	1.845e-011
S_B	β_{DC}	1.668 ± 0.103	2.886 ± 0.684	3.022e-006

not much dramatically. This means breath became more harmonic in case of healthy group when pressure on lower limbs occurred. Parameter p_3 perfectly separates proband groups except for one proband (number 15). His breath is showed in figure 5.2 and it is clear that this breath course is outlayer for healthy group. Parameter β_{DC} on the other hand stays low for healthy group and is higher for pathological group. It is significant for both measured situations although for situation S_B it is again very significant as β_{DC} decreased for C_1 and increased for C_2. Box plotted values for these two parameters follows for illustration:
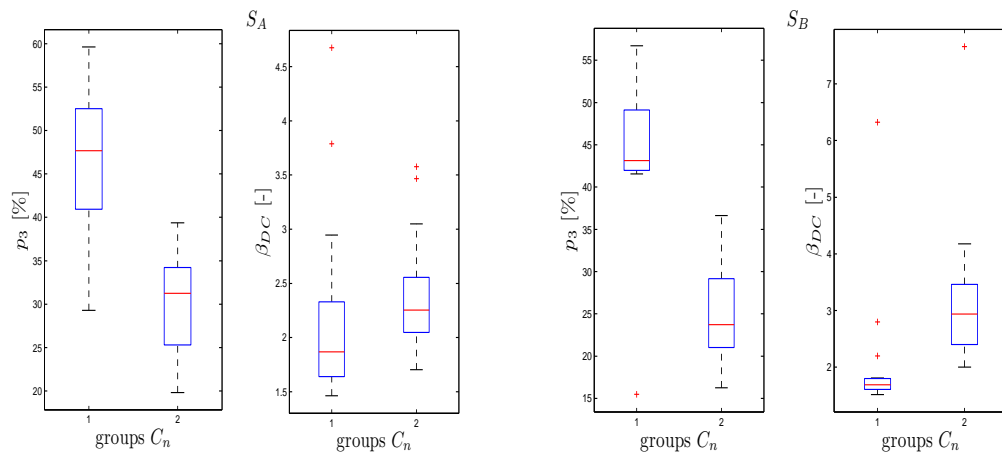
FIGURE 5.1: Box plots of p_3 and β_{DC} for situations S_A and S_B. They show significant difference between proband groups.

Red crosses in box plots stands for outlayers out of the range defined in 3.4.4.1. We will look on properties of breath-curves of these proband closer. In a table 5.2 proband numbers and features values are stated.

TABLE 5.2: Here we show and discuss outlayes properties from harmonicity objectification properties (p_3 and β_{DC}).

	Feature	C_1	C_2	Feature	C_1	C_2
S_A	β_{DC}	07 (4.6739) 08 (3.7877)	21 (3.4672) 29 (3.5771)	p_3		
S_B	β_{DC}	13 (2.1992) 14 (2.8008) 15 (6.3217)	19 (7.6558)	p_3	15 (15.466)	

Box plots (fig. 5.1) and graphs (5.2) examination show that parameter p_3 has quite small value for breath like No. 7 and 8 on fig. 5.2. This breath isn't much harmonic but looks like good breath course. Actually breath courses No. 15 and 19 doesn't have much different values of p_3 and β_{DC} parameters. It is medical question whether breaths courses like No. 7 and 8 are good. If yes then some more effort should be headed to harmonicity of a breath rating for these marginal courses.
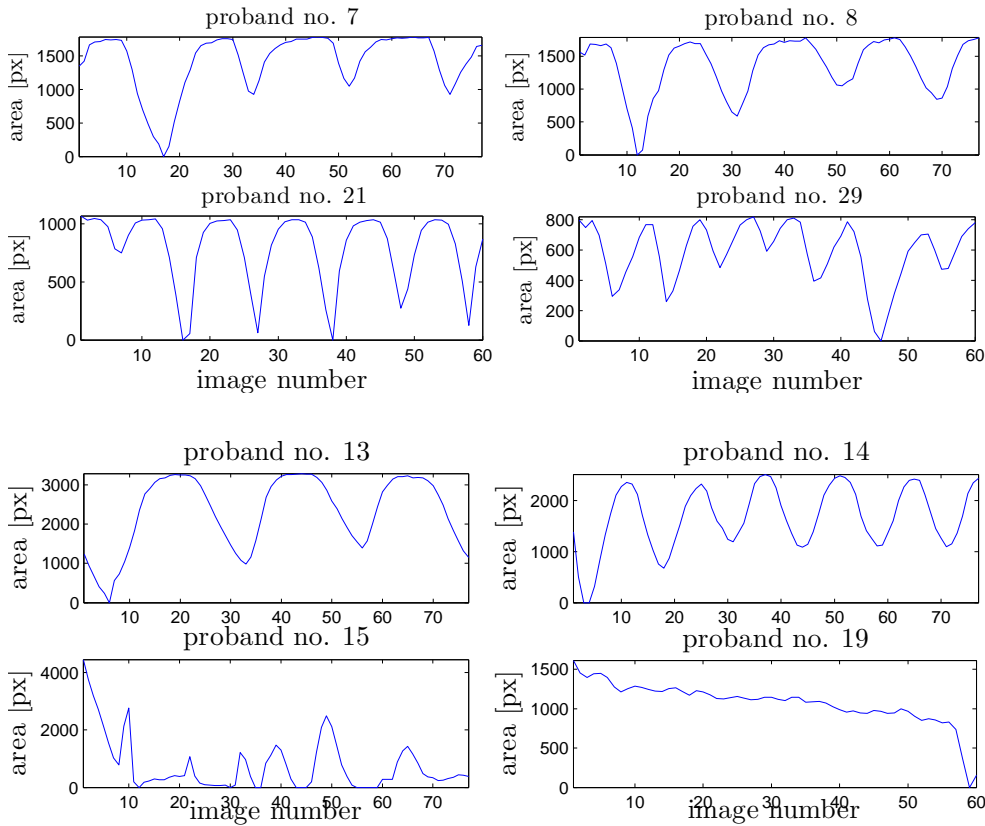
FIGURE 5.2: This figure shows breath-curve of outlayers which are visible as red crosses on box plots in fig. 5.1. Upper part of figure shows breath-curves from S_A and lower half shows curves from S_B.

5.2.2 Res- and pos-curve frequencies and amplitudes.

Next important parameters are ones describing frequency of a breath and its depth. These parameters are f_r, a_r, f_p, r_{rs} and a_p. Results of measurements follows:

This group of features embodies big statistical significance. The pos-curve amplitude is the only not significantly different parameter on significance level of 0.05 is for. But as discussed in sec. 4.2.2 pos-curve amplitude is dependent on breath curve variance and thus doesn't say much about diaphragm's behaviour as is. More interesting parameter

TABLE 5.3: Statistical Analysis of C_1 and C_2 for breath depth and its frequency.

	Feature	C_1	C_2	p-value
S_A	f_r	0.209 ± 0.060	0.262 ± 0.058	0.015
	a_r	0.095 ± 0.043	0.034 ± 0.014	4.18e-005
	f_p	0.035 ± 0.014	0.050 ± 0.022	0.035
	r_{rs}	0.299 ± 0.196	0.314 ± 0.209	0.837
	a_p	0.022 ± 0.013	0.011 ± 0.007	0.005
	σ_{DC}	0.074 ± 0.031	0.032 ± 0.013	6.37e-5
	γ_{DC}	-0.203 ± 0.568	-0.682 ± 0.244	0.006
S_B	f_r	0.221 ± 0.076	0.358 ± 0.110	4.115e-004
	a_r	0.095 ± 0.047	0.014 ± 0.010	4.593e-006
	f_p	0.044 ± 0.024	0.041 ± 0.015	0.600
	r_{rs}	0.301 ± 0.117	1.220 ± 0.916	0.002
	a_p	0.032 ± 0.020	0.020 ± 0.013	0.045
	σ_{DC}	0.085 ±0.038	0.03 ± 0.024	2.3e-5
	γ_{DC}	-0.009 ± 0.57	-0.567 ± 0.662	0.015

r_{rs} proved as statistically significant. Also pos-curve frequency doesn't embody statistical significance for S_B. As we mentioned sec. 3.4.2.1, pos-curve frequency doesn't describe diaphragm average drift properly and thus serve only as rough insight. The general significance of this group is not as big as in above section but still there are clear and hypothesized differences between proband groups. Situation is clearly visible on fig 5.3.

We assumed that probands with pathological conditions breath faster — have larger res-curve frequency which even more rise when pressure on lower limbs is presented. It points to breath difficulties for pathological group. Also res- pos-curves ratio raises significantly for pathological group and stays still for healthy group. It shows that average position drift of a diaphragm composed larger (r_{rs} in situation S_B for pathological group — value larger then 1 means pos-curve amplitude bigger then res-curve amplitude) part of diaphragms movement then respiratory movement.

5.2.3 Static features statistics

We deal with all the remaining features in this section. These are static features describing diaphragm shape and position. In a relevant table 5.4 statistics are shown for those features. As static features deal with shape and position and not time course they were extracted from all measured situations. Statistical significance was highlighted by color. Green are features with p-value below 0.001 and in blue color are shown features with t-test p-value only below 0.05. Thus in green color are shown features with great statistical significance and thus more strong in the groups differentiation against each other.
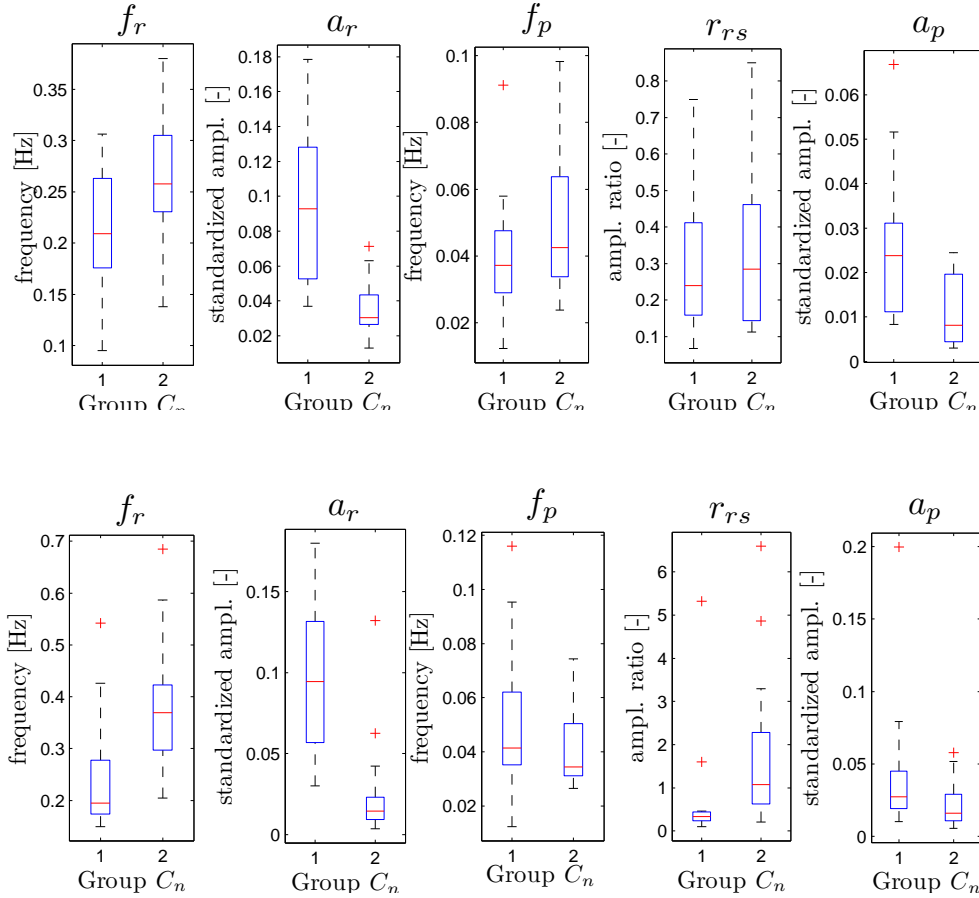
FIGURE 5.3: This figure shows box plots of features stated in table 5.3. Upper part of the figure is for S_A and lower is for S_B.

The most significant inter-group difference occurred in a case of properties h_d and vd_6 i.e. height of an overlapped strip and distance of back partition of diaphragm from back marker. Height of an overlapped strip was almost still during measurements. Although there are differences in significance they are not large and fluctuate around p-value of 0.001. In result healthy people had the strip lower than pathological group. That indicates to flatter diaphragm. Flatness measured by this way didn't changed much through measured situations.

The diaphragm flattering describe also parameters ρ_d and e_d. Parameter ρ_d results are more statistically significant. Statistical significance raised for situation B. It was caused by lowering variance of values for healthy group. This could be caused by unification of diaphragm shape while pressure is present. The mean value slightly raised for group C_2 and lowered for group C_1. Overlapping strip parameter resulted in no great change of diaphragm flatness through situations. Lowering of fitted circle diameter means higher diaphragm. It could be caused by partial change in diaphragms shape and thus smaller circles fitted. Detailed inspection of diaphragms partial shapes would be helpful for

TABLE 5.4: Statistical Analysis of static features is presented here.

	Feature	C_1	C_2	p-value
S_A	h_d	0.256 ± 0.055	0.323 ± 0.053	0.001
	dec_a	23.534 ± 7.133	14.957 ± 5.617	6.57e-004
	dec_r	9.982 ± 8.159	6.842 ± 5.091	0.192
	vd_6	0.212 ± 0.198	-0.401 ± 0.111	1.34e-010
	c_d	0.406 ± 0.059	0.424 ± 0.034	0.294
	ρ_d	0.662 ± 0.112	0.556 ± 0.039	0.002
	e_d	0.801 ± 0.101	0.716 ± 0.068	0.008
	α_2	28.764 ± 6.648	26.512 ± 8.742	0.424
	α_6	7.651 ± 3.503	6.896 ± 3.259	0.539
	b_1	0.150 ± 0.036	0.191 ± 0.041	0.005
	b_2	0.228 ± 0.049	0.286 ± 0.045	0.001
	b_3	0.252 ± 0.065	0.315 ± 0.054	0.005
	b_4	0.222 ± 0.064	0.281 ± 0.056	0.008
	b_5	0.148 ± 0.042	0.204 ± 0.043	8.20e-004
S_B	h_d	0.255 ± 0.051	0.315 ± 0.058	0.003
	dec_a	24.746 ± 9.619	17.802 ± 5.807	0.017
	dec_r	9.341 ± 5.840	12.048 ± 3.745	0.125
	vd_6	0.248 ± 0.139	-0.294 ± 0.120	3.504e-013
	c_d	0.411 ± 0.050	0.416 ± 0.036	0.753
	ρ_d	0.635 ± 0.065	0.565 ± 0.040	9.513e-004
	e_d	0.801 ± 0.078	0.770 ± 0.090	0.304
	α_2	30.559 ± 6.679	21.356 ± 5.331	1.630e-004
	α_6	9.255 ± 5.683	10.041 ± 6.837	0.723
	b_1	0.142 ± 0.039	0.200 ± 0.047	5.691e-004
	b_2	0.227 ± 0.049	0.284 ± 0.053	0.003
	b_3	0.258 ± 0.056	0.312 ± 0.058	0.011
	b_4	0.236 ± 0.049	0.277 ± 0.055	0.029
	b_5	0.163 ± 0.042	0.202 ± 0.041	0.010
S_C	h_d	0.243 ± 0.058	0.323 ± 0.057	4.913e-004
	dec_a	24.279 ± 11.148	20.691 ± 3.768	0.239
	vd_6	0.229 ± 0.272	-0.153 ± 0.117	4.457e-005
	c_d	0.413 ± 0.078	0.388 ± 0.057	0.286
	ρ_d	0.646 ± 0.083	0.562 ± 0.047	0.002
	e_d	0.827 ± 0.120	0.777 ± 0.094	0.209
	α_2	30.667 ± 8.449	27.837 ± 8.091	0.333
	α_6	8.306 ± 5.400	7.926 ± 4.877	0.833
	b_1	0.137 ± 0.039	0.205 ± 0.062	7.591e-004
	b_2	0.227 ± 0.049	0.287 ± 0.063	0.006
	b_3	0.258 ± 0.066	0.324 ± 0.052	0.004
	b_4	0.230 ± 0.068	0.291 ± 0.054	0.009
	b_5	0.156 ± 0.069	0.207 ± 0.034	0.017

future work.

Inspecting parameter vd_6 shows that healthy group has diaphragm leid higher than pathological group. When pressure on lower limbs occurred diaphragm lowered even

more. This movement was significantly greater for pathological group. For situation C i.e. pressure on lower limbs while holding breath diaphragm again lowered its position and same as in the previous case the lowering is stronger for pathological group.

Diaphragm declination in caudal position resulted in strongly statistical significant group difference for situation S_A. It shows that healthy group has the dorsal part of diaphragm in lower position then pathological group. It is more significant in diaphragm caudal position. Pathological group tend to have diaphragm more in horizontal position or have the dorsal part of diaphragm higher then ventral. As pressure on lower limbs is applied for situation S_B pathological group tend to rotate diaphragm more to vertical rotation by lowering its dorsal part. Healthy group let the diaphragm almost in the same rotation. This leads to lesser statistically significant difference between groups. For situation S_C this symptoms even more amplify thus there is no statistically significant difference for situation C.

Last significant part of parameters are partial diaphragm heights $b_1 \ldots b_5$. Diaphragm was flatter in all observed points for healthy group. Interesting observation is that during normal breathing the greatest statistical difference was in dorsal part of diaphragm. For situations S_B and S_C the most statistically significant difference moved to ventral part of diaphragm.

Chapter 6

Classification framework

In this chapter automatic patient classification into healthy and pathological class is described. Classification error, sensitivity and specificity were estimated for selected classifiers. PRTools toolbox for Matlab was used for classification processing ([15], http://www.prtools.org/).

Process of classification consists of the following steps:

1. Selecting a feature performance rating method.

2. Choosing a feature selection method.

3. Choosing a classifier.

4. Random dividing feature set into training and testing set.

5. Classifier training.

6. Classification of a testing data set and its parameters estimation.

7. Validation of results by repeating steps 4. – 6. N times.

In the following sections we will briefly present methods used for processing steps 1. – 3. (see 6.1.2). Tests for choosing the best classifier and methods follows after it (6.1.3). Finally we present results — features suitable for patient classification, selected features performance and classification results upon our measured data (6.2).

6.1 Feature selection

Main source of information for classification work was [15]. Classifiers and classification basics are well described in [16]. Source of information about float feature selection was used [17].

6.1.1 Experimet settings

Evaluation of a feature performance and following feature selection was performed on the whole data set. Due to its small size, problems in a precision of performance evaluation occurred for smaller data subsets. First $\frac{inter}{intra}$ class distance was used as performance evaluation method. Later tests of other measures were processed. Float forward selection was used for features selection due to its speed and good results.

For every classification turn data were randomly split into training (10 subjects) and testing set (6 (from C_1) resp. 7 (from C_2) subjects). Classification was repeated over 100 runs and classification error, specificity and selectivity were computed. Every whole classification circle was besides repeated 4 times in order to reduce further noise.

The four following classifiers were tested: Support vector machine, Quadratic, Parzen and Normal densities based linear (LDC) classifier. The quality of features were confirmed by performance measures.

6.1.2 Choosing proper feature performance estimation method.

PRTools provide several methods for evaluating feature performance. We chose following measures for testing:

- Sum of squared Euclidean distances — **eucl-s**.

- Minimum of squared Euclidean distances — **eucl-m**.

- $\frac{Inter}{intra}$ class distance — **in-in**.

- Sum of estimated Mahalanobis distances — **maha-s**.

- Minimum of estimated Mahalanobis distances — **maha-m**.

We used LDC classifier for classification of a test data and error rate was used for measuring quality of a performance evaluation method. Up to 8 features were selected for performing classification test.

As the selection method was forward every smaller selected feature set would be subset of any bigger set created with forward method and with respect to order of the features. For example selection of only 2 features with in-in performance evaluation method would result into $\{p_3, b_5\}$). Our attempt resulted in two different sets of 8 features. One for methods in-in, maha-s, maha-m which selected the same set. And second for euclidean methods.

$$(6.1)$$

Set_1 (in-in, maha-s, maha-m methods) = $\{p_3, b_5, \beta_{DC}, dec_r, f_p, \alpha_2, \rho_d, f_r\}$

Set_2 (eucl-s, eucl-m methods) = $\{a_r, \sigma_{DC}, a_p, t_s, p_3, h_d, b_3, b_4\}$

Classification results are shown in figure 6.1.
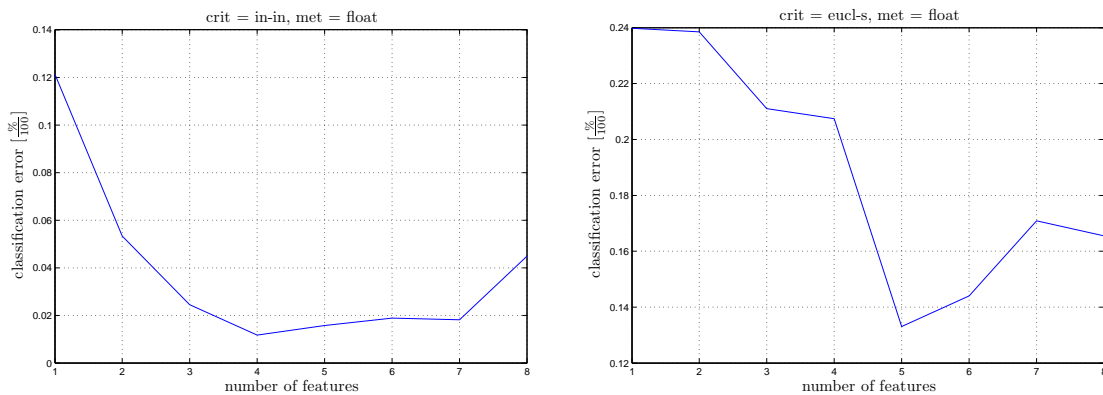
FIGURE 6.1: In this figure we show results of classification performed by LDC classifier and done in order to find the best features performance method. Left image shows classification error for feature set Set_1 (and appropriate subsets) and right image shows the same for Set_2.

Better classification performance was realized among Set_1 selected with usage of one of above stated performance estimation methods. We chose to use $\frac{inter}{intra}$ class distance ratio as main method for performance estimation.

6.1.3 Choosing acceptable selection method for feature selection.

PRTools provide also few feature selection methods. Choosing the best one was aim of test performed among our data. Following method were tested:

- float

- backward

- branch and bound

- plus l takeaway r

LDC classifier was also used for testing selected features performance. We used $\frac{inter}{intra}$ features performance estimation method after tests done in sec. 6.1.2. We use following notation for selected fetures set: $Set_{method-shortcut}(numer-of-features) = \{features-list\}$. Method shortcuts are as follows: f — forward, b — backward, bb — branch and bound, lr — plus r, takeaway l.

▷ **Float method.**

Features selected by float method were already found in proper section (6.1.2). Same rule 6.1 as above applies for shorter sets selection.

$Set_f(8) = \{p_3, b_5, \beta_{DC}, dec_r, f_p, \alpha_2, \rho_d, f_r\}$

▷ **Backward method.**

As backward method picks up features in different way rule 6.1 wasn't complied and thus sets after every step is presented.

$Set_b(1) = \{p_3\}$
$Set_b(2) = \{p_3, \beta_{DC}\}$
$Set_b(3) = \{p_3, \beta_{DC}, b_2\}$
$Set_b(4) = \{f_p, p_3, \beta_{DC}, b_2\}$
$Set_b(5) = \{f_p, p_3, \beta_{DC}, dec_r, b_2\}$
$Set_b(6) = \{f_p, p_3, \beta_{DC}, dec_r, b_1, b_2\}$
$Set_b(7) = \{f_p, p_3, \beta_{DC}, dec_r, b_1, b_2, b_3\}$
$Set_b(8) = \{f_p, p_3, \beta_{DC}, dec_a, dec_r, b_1, b_2, b_3\}$

▷ **Branch and bound method.**

Branch and bound method doesn't complies rule 6.1 thus sets after every step is presented.

$Set_{bb}(1) = \{p_3\}$
$Set_{bb}(2) = \{b_5, p_3\}$
$Set_{bb}(3) = \{\beta_{DC}, b_5, p_3\}$
$Set_{bb}(4) = \{\beta_{DC}, f_p, b_2, p_3\}$
$Set_{bb}(5) = \{\beta_{DC}, dec_r, f_p, h_d, p_3\}$
$Set_{bb}(6) = \{\beta_{DC}, dec_r, f_p, b_1, b_2, p_3\}$
$Set_{bb}(7) = \{\beta_{DC}, dec_r, f_p, e_d, b_1, b_2, p_3\}$
$Set_{bb}(8) = \{\beta_{DC}, dec_r, f_p, e_d, b_3, b_1, b_2, p_3\}$

▷ **Plus l takeaway r method.**

We tested this method for different l and r values. We don't have enough space to show all produces sets so we will show only classification outcomes in next part of a section. Also we use following notation for this method l and r values: LR_{lr} l and r values are put in the subscript. We found some redundancy in results as the same sets was given by different LR settings and above stated methods. Resulting set by LR_{10} was the same as by *float* method.

Resulting set by LR_{53} was the same as by *backward* method. Two more results as an example follows:

$Set_{LR30}(1) = \{p_3\}$
$Set_{LR30}(2) = \{p_3, b_5\}$
$Set_{LR30}(3) = \{p_3, \beta_{DC}, b_5\}$
$Set_{LR30}(4) = \{p_3, \beta_{DC}, dec_r, b_5\}$
$Set_{LR30}(5) = \{f_p, p_3, \beta_{DC}, dec_r, b_5\}$
$Set_{LR30}(6) = \{p_3, \beta_{DC}, b_5, f_p, dec_r, \alpha_2\}$
$Set_{LR30}(7) = \{f_p, p_3, \beta_{DC}, dec_r, e_d, b_1, b_2\}$
$Set_{LR30}(8) = \{f_p, p_3, \beta_{DC}, dec_r, e_d, \alpha_2, b_1, b_2\}$

$Set_{LR50}(1) = \{p_3\}$
$Set_{LR50}(2) = \{p_3, \beta_{DC}\}$
$Set_{LR50}(3) = \{p_3, \beta_{DC}, h_d\}$
$Set_{LR50}(4) = \{f_p, p_3, \beta_{DC}, h_d\}$
$Set_{LR50}(5) = \{f_p, p_3, \beta_{DC}, h_d, dec_r\}$
$Set_{LR50}(6) = \{f_p, p_3, \beta_{DC}, dec_r, b_1, b_2\}$
$Set_{LR50}(7) = \{f_p, p_3, \beta_{DC}, dec_r, b_1, b_2, b_3\}$
$Set_{LR50}(8) = \{f_p, p_3, \beta_{DC}, dec_a, dec_r, b_1, b_2, b_3\}$

Classification performances are shown on the following figures 6.2 and 6.3. Every feature selection method gave us analogous results only differing in the number of features achieving the best classification. The best result of classification error is stated in tab 6.1.

The best classification resulted from methods *float* and LR_{10} which actually gave us the same result. Best classification was achieved for 4 features long following subset $\{f_p, p_3, \beta_{DC}, b_2\}$. As figures 6.2 and 6.3 and table 6.1 shows, every method gave us

TABLE 6.1: The best classification error achieved by various feature selection methods in order to analyse its efficiency.

Method	Float	Back.	B & B	LR_{10}	LR_{30}	LR_{50}	LR_{53}
The best class. err.	0.012	0.011	0.013	0.01	0.014	0.013	0.012
No. of features needed	4	7	6	4	5	7	7

similar error achieved for the best classification error. By comparison of subset related to best methods results:

$Set_{LR50}(7) = \{f_p, p_3, \beta_{DC}, dec_r, b_1, b_2, b_3\}$

$Set_{LR30}(5) = \{f_p, p_3, \beta_{DC}, dec_r, b_5\}$

$Set_{bb}(6) = \{\beta_{DC}, dec_r, f_p, b_1, b_2, p_3\}$

$Set_b(7) = \{f_p, p_3, \beta_{DC}, dec_r, b_1, b_2, b_3\}$

$Set_f(8) = \{p_3, b_5, \beta_{DC}, dec_r\}$

These 8 features — $f_p, p_3, \beta_{DC}, dec_r, b_1, b_2, b_3, b_5$ — create complete list of distinct features in above sets. Although different sorting and selection occurs, these features gave us the strongest classification performance. We see that our proposed harmonicity parameters occurs there. Also $b_1 \dots b_5$ parameters which relates to diaphragm height are present. Also pos-curve frequency and diaphragm declination. These parameters gave us possibility for good inter class differentiation in situation S_A thus bigger focus could lead to them.

6.2 Results

Resulting from above sections, following settings for our classification tests was used:

- Features performance evaluation method: $\frac{inter}{intra}$ **class distance**.

- Features selection method: **float**.

- Tested classifiers: **LDC, Support vectors, Quadratic, Parzen classifier**.

Feature sets selected for every situation:

S_A feature selection:

$Set_f(8) = \{p_3, b_5, \beta_{DC}, dec_r, f_p, \alpha_2, \rho_d, f_r\}$ Rule 6.1 is again applied here.

S_B feature selection:

$Set_f(1) = \{p_3\}$

$Set_f(2) = \{p_3, \beta_{DC}\}$
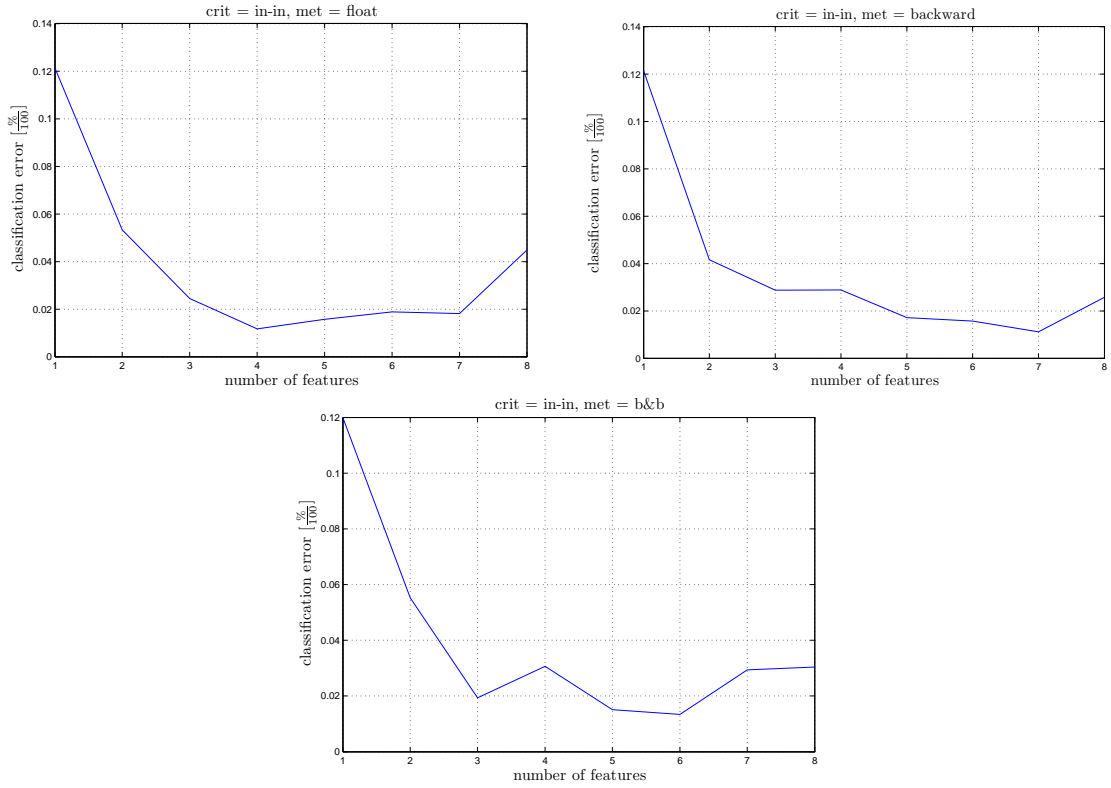
FIGURE 6.2: Comparison of different methods for feature selection. Every method gave us similar result but every for different number of features. The float method was picked up for further data classification for its speed and the smallest number of features to reach minimal classification error.

$Set_f(3) = \{p_3, \beta_{DC}, c_d\}$

$Set_f(4) = \{p_3, \beta_{DC}, c_d, dec_a\}$

$Set_f(5) = \{p_3, \beta_{DC}, c_d, dec_a, \sigma_{DC}\}$

$Set_f(6) = \{p_3, \beta_{DC}, c_d, dec_a, \sigma_{DC}, \alpha_6\}$

$Set_f(7) = \{p_3, \beta_{DC}, c_d, dec_a, \sigma_{DC}, \alpha_6, f_r\}$

$Set_f(8) = \{p_3, \beta_{DC}, \sigma_{DC}, b_1, b_5, \gamma_{DC}, dec_r, f_r\}$

S_C feature selection:

$Set_f(1) = \{b_1\}$

$Set_f(2) = \{b_1, dec_r\}$

$Set_f(3) = \{dec_r, c_d, b_5\}$

$Set_f(4) = \{dec_r, c_d, b_5, e_d\}$

$Set_f(5) = \{dec_r, c_d, b_5, e_d, h_d\}$

$Set_f(6) = \{dec_r, c_d, b_5, e_d, h_d, \rho_d\}$

$Set_f(7) = \{dec_r, c_d, b_5, e_d, \rho_d, b_4, b_3\}$

FIGURE 6.3: Comparison of Plus l minus r feature selection method for different inputs. The best results came from basic settings l = 1, r = 0. The result was the same as by float method (pictured above on fig 6.2.)

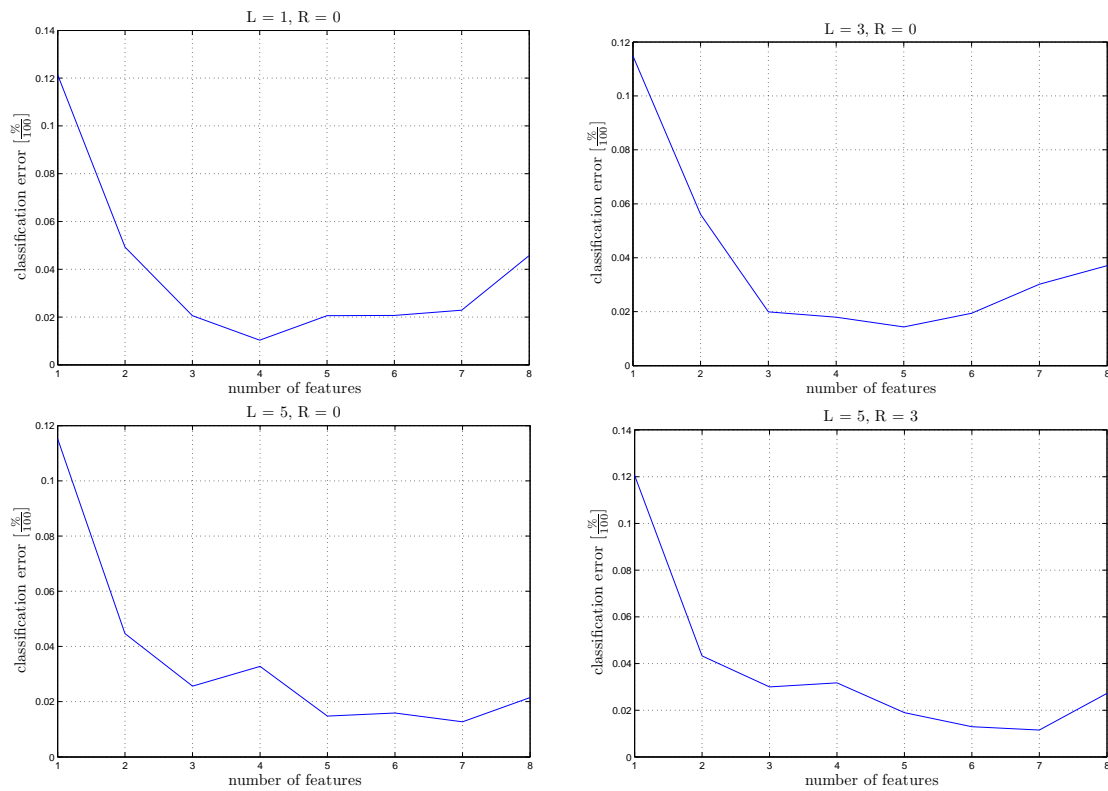$Set_f(8) = \{dec_r,\, c_d,\, b_5,\, e_d,\, b_4,\, b_3,\, \rho_d,\, b_1\}$

Results for situations A — C follows:

6.2.1   Situation A

TABLE 6.2: Results on training and testing sets: S_A

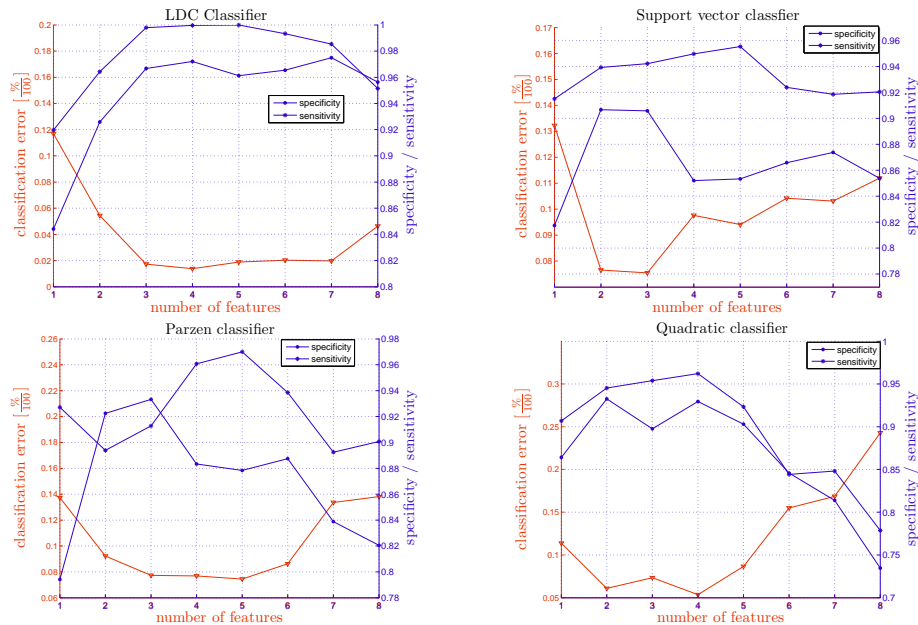|	Support vector classifier			Quadratic classifier		
	spec.	sens.	error	spec.	sens.	error
S_1	0.817	0.915	0.132	0.864	0.907	0.114
S_2	0.907	0.939	0.077	0.932	0.945	0.061
S_3	0.906	0.942	0.075	0.897	0.954	0.073
S_4	0.852	0.950	0.098	0.930	0.962	0.054
S_5	0.853	0.955	0.094	0.903	0.923	0.087
S_6	0.866	0.924	0.104	0.846	0.844	0.155
S_7	0.874	0.919	0.103	0.814	0.848	0.168
S_8	0.854	0.920	0.112	0.735	0.779	0.243
	Parzen classifier			LDC		
	spec.	sens.	error	spec.	sens.	error
S_1	0.794	0.927	0.137	0.844	0.920	0.117
S_2	0.922	0.894	0.092	0.926	0.964	0.054
S_3	0.933	0.913	0.077	0.967	0.998	0.017
S_4	0.883	0.961	0.077	**0.972**	**1.000**	**0.014**
S_5	0.878	0.970	0.074	0.961	1.000	0.019
S_6	0.887	0.939	0.086	0.965	0.993	0.020
S_7	0.839	0.892	0.134	0.975	0.985	0.020
S_8	0.820	0.901	0.138	0.956	0.951	0.046

FIGURE 6.4: Classification tests for different classifiers among the S_A data. LDC calssifier achieved the best result.

TABLE 6.3: Results on training and testing sets: S_B

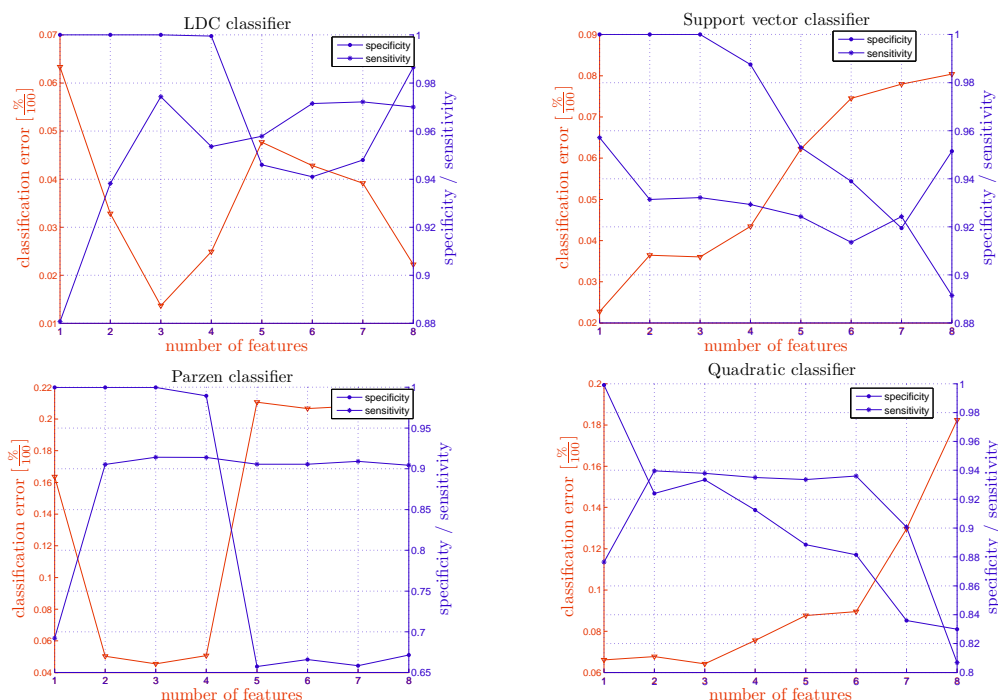|	Support vector classifier			Quadratic classifier		
	spec.	sens.	error	spec.	sens.	error
S_1	1.000	0.957	0.023	0.999	0.876	0.066
S_2	1.000	0.931	0.036	0.924	0.940	0.068
S_3	1.000	0.932	0.036	0.933	0.938	0.064
S_4	0.987	0.929	0.043	0.912	0.935	0.076
S_5	0.953	0.924	0.062	0.888	0.934	0.088
S_6	0.939	0.914	0.075	0.881	0.936	0.090
S_7	0.919	0.924	0.078	0.836	0.901	0.130
S_8	0.951	0.891	0.080	0.830	0.807	0.182
	Parzen classifier			LDC		
	spec.	sens.	error	spec.	sens.	error
S_1	1.000	0.692	0.164	1.000	0.881	0.063
S_2	1.000	0.905	0.050	1.000	0.938	0.033
S_3	1.000	0.914	0.046	**1.000**	**0.974**	**0.014**
S_4	0.989	0.914	0.051	1.000	0.954	0.025
S_5	0.657	0.906	0.211	0.946	0.958	0.048
S_6	0.666	0.906	0.207	0.941	0.971	0.043
S_7	0.658	0.909	0.208	0.948	0.972	0.039
S_8	0.671	0.904	0.205	0.986	0.970	0.022

FIGURE 6.5: Classification tests for different classifiers among the S_B data. The best classifiers was LDC — same as for situation A.

TABLE 6.4: Results on training and testing sets: S_C

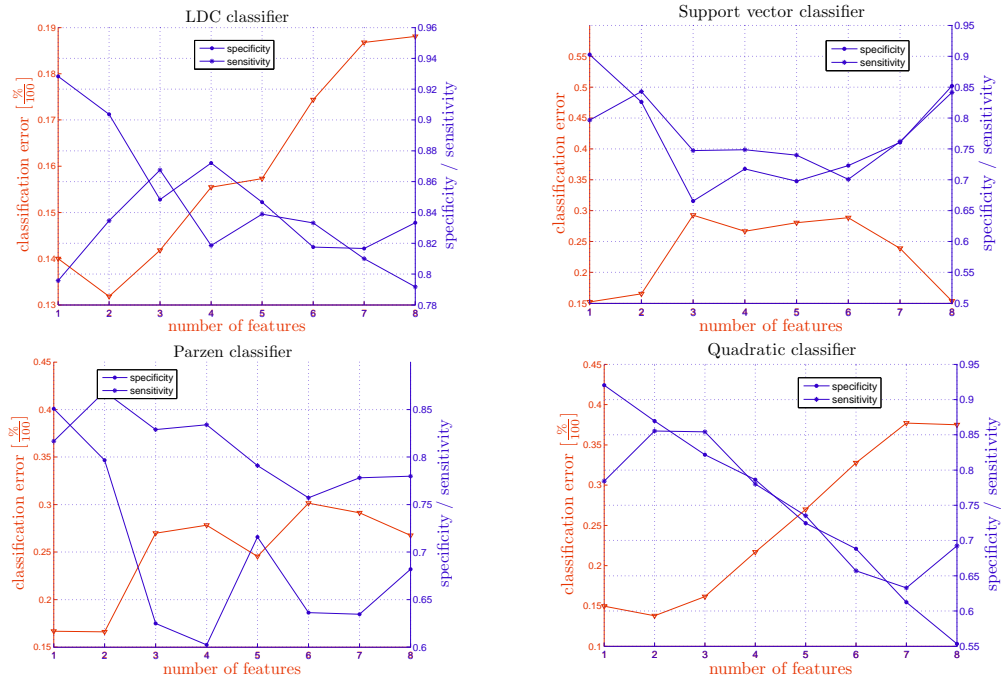|	Support vector classifier			Quadratic classifier		
	spec.	sens.	error	spec.	sens.	error
S_1	0.902	0.796	0.152	0.920	0.784	0.150
S_2	0.826	0.843	0.165	**0.870**	**0.855**	**0.138**
S_3	0.665	0.747	0.292	0.822	0.854	0.162
S_4	0.718	0.749	0.266	0.786	0.780	0.217
S_5	0.698	0.740	0.281	0.725	0.735	0.270
S_6	0.723	0.701	0.289	0.688	0.657	0.328
S_7	0.760	0.762	0.239	0.613	0.633	0.377
S_8	0.852	0.841	0.153	0.553	0.692	0.375
	Parzen classifier			LDC		
	spec.	sens.	error	spec.	sens.	error
S_1	0.851	0.817	0.167	0.928	0.796	0.140
S_2	0.797	0.869	0.166	**0.904**	**0.835**	**0.132**
S_3	0.625	0.829	0.270	0.848	0.867	0.142
S_4	0.602	0.834	0.278	0.872	0.819	0.155
S_5	0.716	0.791	0.245	0.847	0.839	0.157
S_6	0.636	0.757	0.301	0.817	0.833	0.174
S_7	0.635	0.778	0.291	0.817	0.810	0.187
S_8	0.682	0.780	0.267	0.833	0.792	0.188

FIGURE 6.6: Classification tests for different classifiers among the S_C data. This data set was harder to separate by classification. Quadratic and LDC classifiers reached similar classification error. Quadratic classifier had smaller specificity and littler higher sensitivity then LDC classifier.

6.2.2 Conclusion

First we empirically chose $\frac{inter}{intra}$ class distance ratio as the best method for feature performance estimation. $\frac{inter}{intra}$ class distance along with mahalanobis distance provided the best feature selection which was verified by classification error evaluation. Second we picked up *float* method for the feature selection. See [17] for method details. Classification of a data set composed by features chosen with the float selection method gave us small classification error values for the smallest feature subsets. And computation time is also short within usage of this method.

Using $\frac{inter}{intra}$ class distance ratio for feature performance estimation and $float$ method for feature selection gave us these features selected in different situations. We present only subsets with biggest classification performance during subsequent classification:

A: $Set_f(4) = \{p_3, b_5, \beta_{DC}, dec_r\}$
B: $Set_f(3) = \{p_3, \beta_{DC}, c_d\}$
C: $Set_f(2) = \{b_1, dec_r\}$

Normal Bayesian classifier showed as the best classification choice. A performance analysis using sensitivity and specificity measures with regards to number of selected features was carried out - see Figures 6.4, 6.5 and 6.6. For situation A the worst case when just a unique feature and Parzen classifier are used, the specificity is close to 0.8, sensitivity to 0.93. On the contrary, the best performance is achieved using LDC classifier and feature combination $Set_f(4)$ achieving sensitivity 0.97, specificity 1.0 and classification error 0.014. For situation B specificity and sensitivity have their smallest values 0.66 for specificity and 0.7 for sensitivity again with Parzen classifier. LDC classifier raise up to 1 for specificity and 0.974 for selectivity and 0.014 for classification error with $Set_f(3)$ feature subset. Situation C showed to be the hardest classification case. Specificity and sensitivity decreased to 0.55 resp. 0.63 for their worst cases in a case of quadratic classifier with $Set_f(8)$ subset. Better results were achieved for smaller amounts of features: it was classification error 0.132 for LDC classifier and 0.138 for quadratic classifier with feature subset $Set_f(2)$. Specificity and sensitivity was 0.9 resp. 0.84 for LDC classifier. All results summarizes tables 6.2, 6.3 and 6.4.

Chapter 7

Conslusion

7.1 Conclusion

Main goal of the presented work was to devise methodology for diaphragm inspection and inter healthy and pathological groups comparison. Proposed methods were able to characterize both diaphragm's motion and position along with shape. Motion parametrization introduced separation of a diaphragm's motion onto respiration and postural part. Possibilities of breath assessment by FFT spectrum and statistical moments processing was accomplished. Statistical methods includes measurement of diaphragm's flatness, rotation, partial and overall height.

As a result group of people with structural spine finding and pain present in back area was compared with group of healthy people. Significant differences between groups were confirmed. Most significant parameters were those characterizing harmonicity of a breath's shape, breath's frequency and amplitude. As was hypothesized statistical significance of differences between groups rose for situation with pressure applied on lower limbs.

Last part of the work dealt with possibilities of automatic patient assessment. Also diaphragm parameters' performance was evaluated by classification methods. Classification results of data are related to their statistical significance. This relation evoked that features performance evaluation confirmed the same features significancy as we stated in the previous paragraph. Classification error rate was following: for S_A and S_B it was the same — 0.014, for S_C it was 0.13 or 0.14 depending on used classifier.

7.2 Future work suggestions

The main aim of a future research would be confirmation of study conclusions on a bigger population sample. Testing or training groups consisting of 16 resp. 17 probands aren't very satisfactory groups sizes for statistical conclusions. Future development of classification framework leading to prediction of intervertebral disc prolapse is also considered future enhancement of this methodology.

Automatic detection of a diaphragm contour could lead to more precise results. More effort would be useful in pos- curve processing — generalized parametrization should be proposed to objectify the complex curve shape.

For dynamical parameters we mentioned adaptive filtration would be possible approach for pos-curve extraction. Also res-curve processing could be improved as an aim of future line of research. We proposed FFT spectrum for signal processing but more approaches for spectral assessment could be used. There are limitations with resolution on lower frequencies, some methods for resolution enhancement would be helpful. Also focus of other works could lead to time changes of parameters like frequency fluctuations through breath cycle. As for central moments there could be some inaccuracies due to big pos/res-curve amplitude ratio. Subtraction of diaphragm average drift or some robust computing approach could be proposed.

As static parameters are more plain there isn't much effort to do. Some extention could be added to ellipse and circle fitting as we are afraid that their results suffer from noise present through not accurate curves fitting.

Diaphragm objectification is complex and interesting theme which would deserve strong methodical basis. Thus we tried to point out as much remarks as we were able to find out after doing an overview of our processed effort.

Bibliography

[1] T. Rychnovský. *MRI respirační dynamiky a posturální funkce bránice.* PhD thesis, Charles University in Prague, Faculty of Physical Education and Sport, 2010.

[2] P. Paclik et al. R.P.W. Duin, P. Juszczak. *PRTools4, A Matlab Toolbox for Pattern Recognition.* Delft Pattern Recognition Research, Faculty EWI - ICT, Delft University of Technology, P.O. Box 5046, 2600 GA Delft, The Netherlands, August 2007. PRTools version 4.1.

[3] D. Gierada, J. Curtin, S.Erickson, R. Prost, J. Strandt, and L. Goodman. Diaphragmatic motion: Fast gradient-recalled-echo mr imaging in healthy subjects. *Radiology*, pages 879–884, 1995.

[4] A. Gauthier, S. Verbatick, M. Estenn, C. Segebartg, P. Macklem, and M. Paiva. Three-dimensional reconstruction of the in vivo human diaphragm shape different lung volume. *J Appl Physiol*, pages 495–506, 1994.

[5] P. Cluzel, T. Similowski, C. Chartrand-Lefebvre, M. Zelter, J. Derenne, and P. Grenier. Diaphragm and chest wall: assessment of the inspiratory pump with mr imaging-preliminary observations. *Radiology*, pages 574–583, 2000.

[6] K. Suga, T. Tsukuda, and H. Awaya. Impaired respiratory mechanics in pulmonary emphysema: evaluation with dynarmic breathing mri. *J Magn Reson Imaging*, pages 510–520, 1999.

[7] R. Takazakura, M. Takahashi, N. Nitta, S. Sawai, N. Tezuka, S. Fujino, and K. Murata. Assessment of diaphragmatic motion after lung resection using magnetic resonance imaging. *Radiat Med*, (4):155–163, 2007.

[8] S. Kiryu, S. Loring, Y. Mori, N. Rofsky, H. Hatabu, and M.Takahashi. Quantitative analysis of the velocity and synchronicity of diaphragmatic motion: dynamic mri in different postures. *Magn Reson Imaging*, (10):1325–32, 2006.

[9] P. Kolar, J. Neurwith, J. Sanda, V. Suchanek, Z. Svata, J. Volejnik, and M. Pivec1. Analysis of diaphragm movement during tidal breathing and during its activation

while breath holding using mri synchronized with spirometry. *Physiol Res*, (3): 383–392, 2009.

[10] Petr Pollák Pavel Sovka. *Vybrané metody číslicového zpracování signálů.* Vydavatelství ČVUT, Thákurova 1, 160 41 Praha 6, 2003. ISBN 80-01-02821-6.

[11] V. Čížek. *Diskrétní Fourierova Transformace a její použití.* SNTL, Praha, 1981.

[12] R. W. Oppenheim, A. V. Shafer. *Discrete-Time Signal Precessing (2nd edition).* Prentice Hall, Inc., Englewood Cliffs, New Jersey, 1999. ISBN 0-13-083443-2.

[13] Jan Flusser Radim Halíř. Numerically stable direct least squares fitting of ellipses. Technical report, Department of Software Engineering, Charles University in Prague, 1998.

[14] Jiří Militký Milan Meloun. *Kompendium statistického zpracování dat, metody a řešené úlohy.* Academia, Legerova 61, 120 00 Praha 2, 2002. ISBN 80-200-1008-4.

[15] R.P.W.; de Ridder D. van der Heijden, F.; Duin. *Classification, Parameter Estimation and State Estimation - An Engineering Approach Using MATLAB.* John Wiley & Sons Ltd, The Atrium, Southern Gate, Chichester, West Sussex PO19 8SQ, England, 2004. ISBN 0-470-09013-8.

[16] Andrew R. Webb. *Statistical Pattern Recognition, second edition.* John Wiley & Sons Ltd, The Atrium, Southern Gate, Chichester, West Sussex PO19 8SQ, England, 2002. ISBN 0-470-84514-7.

[17] J. Novovicova J. Kittler P. Pudil, F. J. Ferri. Floating search methods for feature selection with nonmonotonic criterion functions. *Proceedings of the Twelfth International Conference on Pattern Recognition.*, Jerusalem: IAPR:279 – 283, 1994.